PHYSICAL REVIEW B **68**, 125104 (2003)

Localization effects and inelastic scattering in disordered heavy electrons

M. C. O. Aguiar,[1] E. Miranda,[1] and V. Dobrosavljević[2]
[1]*Instituto de Física Gleb Wataghin, Unicamp, C.P. 6165, Campinas, SP 13083-970, Brazil*
[2]*Department of Physics and National High Magnetic Field Laboratory, Florida State University, Tallahassee, Florida 32306, USA*
(Received 12 February 2003; revised manuscript received 17 June 2003; published 11 September 2003)

We study ground-state and finite-temperature properties of disordered heavy fermion metals by using a generalization of dynamical mean-field theory which incorporates Anderson localization effects. The emergence of a non-Fermi-liquid metallic behavior even at moderate disorder is shown to be a universal phenomenon resulting from local density of states fluctuations. This behavior is found to have a character of an electronic Griffiths phase, and can be thought of as a precursor of Anderson localization in a strongly correlated host. The temperature dependence of the conducting properties of the system reveal a non-trivial interplay between disorder and inelastic processes, which are reminiscent of the Mooij correlations observed in many disordered metals.

DOI: 10.1103/PhysRevB.68.125104 PACS number(s): 71.27.+a, 72.15.Rn, 71.10.Hf, 75.20.Hr

I. INTRODUCTION

The interplay of disorder and strong correlations remains one of the least understood topics of contemporary condensed matter physics. These effects are believed to bear relevance to many problems that have attracted recent attention, such as the metal-insulator transition (MIT) in two-dimensional electron systems.[1] Disorder effects are also likely to be important for the understanding of the puzzling non-Fermi -liquid (NFL) behavior of several heavy fermion compounds.[2] In some of these systems, impurities seem to play only a subsidiary role: the explanation for the anomalous behavior is more likely to be found in the physics of quantum criticality,[3–7] even though a complete description is still lacking.[8–11] However, in other heavy fermion systems, disorder seems to play a more essential role and seems to be at the origin of the NFL behavior.[12–15]

Several attempts have been made to address theoretically the role of disorder in heavy fermion compounds (see an overview below). Many experimental results can be described within the so-called Kondo disorder model (KDM)[13] or, equivalently, the dynamical mean field theory (DMFT) of disordered Kondo/Anderson lattices,[16,17] at least above the lowest temperatures. Essential to this description is the consideration of the full distribution of local Kondo temperatures T_K. For sufficient disorder, it has a large weight as $T_K \to 0$ describing the presence of dilute low-T_K spins that dominate the thermodynamic and transport properties. However, the KDM/DMFT predictions relied on a fine tuning of the bare disorder that suggested that a more accurate microscopic foundation was necessary. Conspicuously missing in this scheme were fluctuations in the conduction electron local density of states (DOS), a quantity that is crucial for the determination of T_K. This was remedied by two of us through a generalization of the DMFT that incorporates such Anderson localization effects while keeping its local treatment of correlations.[18,19] As a result, the question of the extreme sensitivity to the bare disorder was solved. One important result of this study is the emergence of a power-law distribution of Kondo temperatures $P(T_K) \propto T_K^{\alpha-1}$, where α depends continuously on the strength of disorder W and decreases as W is increased. As the distribution becomes more singular, several thermodynamic quantities become divergent, in a manner characteristic of Griffiths phases.[20] The system eventually localizes at a critical disorder strength W_{MIT}. Since there is no magnetic phase transition this has been dubbed an electronic Griffiths phase.

This initial work[18,19] employed the slave boson large-N theory[21,22] to solve the auxiliary single-impurity problems posed by the method. While versatile, powerful and yet computationally cheap, this approach presents some disadvantages, the main one being the difficulty of working at finite temperatures. It should be reminded that, since we deal with wide distributions of T_K, we need to be able to describe well the full crossover from $T \ll T_K$ to $T \gg T_K$, which is not possible with the slave boson large-N treatment. In particular, conspicuously missing are inelastic scattering processes. In addition, though giving a good description of the low-energy Fermi-liquid regime of the single-impurity problem, this treatment does not incorporate high- and intermediate-energy incoherent processes. Another impurity solver is therefore needed to assess the importance of these intrinsically finite-T and finite-energy features. A particularly useful method, able to fill this gap at a reasonable computational cost, is second order perturbation theory in U. We have used this method to both complement and crosscheck the slave boson results.

In addition to the results of the initial work,[18,19] which have been confirmed by both methods, some of our main conclusions are: (i) there is a subtle interplay between conduction and f-electron site disorder that leads to a surprising *nonmonotonic* dependence of the conducting properties on disorder, a feature that is likely unique to Kondo/Anderson as opposed to Hubbard models, (ii) localization effects are essential for the determination of the distribution of Kondo temperatures and a KDM/DMFT description is clearly insufficient, especially if one starts from an experimentally measured discrete distribution, and (iii) the interplay between disorder and inelastic processes can lead to a temperature dependence of the conducting properties that is reminiscent of the ones found by Mooij and others in several strongly correlated disordered metals.[23] This paper is organized as follows. We review the disorder-based mechanisms of non-

 ©2003 The American Physical Society

Fermi- liquid behavior in the following. Section II describes the model of disordered Anderson lattices we studied and the methods we employed to solve it. Section III focuses on the detailed results obtained within the slave boson large-N method. This expands considerably on the previously published results.[18,19] In Sec. IV, we show the results obtained with perturbation theory. Finally, we wrap up with a general discussion of the strengths and limitations of this study and point out possible future directions in Sec. V. Some details of the computational procedures are given in the Appendix.

In the following we give a brief overview of disorder-based mechanisms of non-Fermi-liquid behavior.

(1) *Kondo-disorder models and the electronic Griffiths phase.* The KDM was proposed early on to account for the temperature dependence of the Cu nuclear magnetic resonance (NMR) linewidths in $UCu_{5-x}Pd_x$ $(x=0.5-1)$.[13] It assumed that disorder in a heavy fermion system generates random spatial fluctuations of the exchange coupling constant J between local moments and conduction electrons (the Kondo coupling). Each local moment was assumed to undergo the Kondo effect in a manner that is completely uncorrelated with the others and each with a characteristic energy scale, its Kondo temperature T_K. Even narrow Kondo coupling distributions lead to a wide distribution of Kondo temperatures due to the latter's exponential dependence on the former. As a result, at low temperatures, many spins are quenched while a few percent remain unquenched and dominate, giving rise to singular, NFL thermodynamic properties (specific heat and magnetic susceptibility). The NMR results in $UCu_{5-x}Pd_x(x=0.5-1)$ are well described within this picture if the distribution function $P(T_K)$ is such that $P(T_K \rightarrow 0) \rightarrow$ const.[13] The KDM gained a natural theoretical setting within the DMFT[24] of a disordered Anderson/Kondo lattice.[16,17] In this approach, each conduction electron site exchanges single particle excitations with an average ''cavity'' bath, which is in turn self-consistently determined. This treatment becomes exact in the limit of infinite dimensionality and is the natural generalization of the Curie-Weiss mean-field theory of magnets to a fermionic system. Its treatment of disorder is equivalent to the well-known coherent potential approximation (CPA).[25] In an Anderson lattice description, the localized f electron is hybridized with its adjacent conduction electron orbital and spatial fluctuations are preserved through the random distribution of hybridization strengths. The local moments are no longer independent since their distribution self-consistently determines the cavity bath. In addition to showing that the KDM corresponds to a rigorous limit of a microscopic Hamiltonian, the DMFT enabled the calculation of other properties such as the resistivity,[16,17] dynamic magnetic susceptibility,[17] optical conductivity,[26] and magneto-resistance,[27] with good agreement with experiments. The non-Fermi-liquid behavior of these quantities hinged on the condition that $P(T_K \rightarrow 0) \rightarrow$ const. Subsequent experiments of muon spin rotation[28] and NMR in high fields[29] showed some inconsistencies with the KDM/DMFT, suggesting that intersite correlations, which are absent from that approach, may play a crucial role at the lowest temperatures. However, annealing studies have further emphasized that the consideration of disorder effects is indispensable.[30]

Despite its success, the KDM/DMFT description suffered from a basic deficiency, which can be ascribed to its extreme sensitivity to the bare disorder distribution. Indeed, the connection between the distribution of J and the distribution of Kondo temperatures is too rigid and a proper description always relies on fine tuning. In particular, discrete distributions of bare parameters can never generate a $P(T_K)$ such that $P(T_K \rightarrow 0) \rightarrow$ const. Likewise, power law distributions of T_K are often necessary and it is not clear how they can be obtained within the KDM/DMFT.

More recently, two of us have pointed out that this can be solved through the inclusion of localization effects. From a basic theoretical point of view, the importance of this modification is unquestionable. Disorder scatters the conduction electrons giving rise to spatial fluctuations in their wave function amplitude. These Anderson localization precursor effects in turn give rise to fluctuations of the conduction electron local DOS. The Kondo temperatures are exponential functions of the local DOS and will show a wide distribution for mild disorder strengths, *even in the absence of fluctuations in J*.[31] In addition, direct experimental determination of the distribution of J from x-ray absorption fine-structure (XAFS) experiments in $UCu_{5-x}Pd_x$ have shown that additional conduction electron disorder is necessary for the interpretation of the results within the KDM/DMFT.[32,33] Finally, the addition of localization effects has proved to be just the necessary ingredient for the elimination of the extreme sensitivity to the bare disorder and for a much more universal description.

The average cavity bath of the DMFT, however, completely neglects DOS fluctuations and a more general treatment is necessary. Progress could be made by means of the statistical dynamical mean field theory (statDMFT), which incorporates the full distribution of the conduction electron local DOS, while keeping the treatment of local correlations already present in the DMFT.[34,35] The treatment involves solving a fully self-consistent loop: the f-electron fluid gives rise to an effective disorder potential for the conduction electrons, while the latter's DOS fluctuations determine the distribution of Kondo temperatures. We enumerate the main conclusions of our analysis:[18,19]

Universality. The distributions of several physical quantities (Kondo temperatures, local DOS of f and conduction electrons, scattering T matrices) assume a universal log-normal form for weak to moderate disorder, irrespective of the form of the bare distribution. We have verified this for Gaussian, square and discrete bare distributions of conduction electron on-site energies and hybridization strengths. This is in contrast to the KDM/DMFT results and reflects the mixing of many different sites connected by the extended conduction electron wave function.

Electronic Griffiths phase. Increasing the disorder generates wide T_K distributions, leading to a Griffiths phase with non-Fermi-liquid behavior. This Griffiths phase is not tied to any magnetic phase transition but is electronic in origin: it is generated by the precursors to the Anderson localization transition.

Metal-insulator transition. There is an Anderson-type localization transition at a critical value of the conduction electron diagonal disorder.

Nonmonotonic conductivity as a function of the disorder. The typical conduction electron DOS, which vanishes at the localization transition and serves as a measure of the conducting properties shows a counterintuitive nonmonotonic behavior as a function of disorder for a wide range of fillings. This surprising feature originates in the interplay between the bare and the *f*-electron disorder potentials and is tied to the proximity to the Kondo insulating (pseudo)gap.

(2) *Magnetic Griffiths phase scenario.* An alternative theoretical scenario for disorder-induced non-Fermi liquid behavior is the magnetic Griffiths phase.[36–38] In the vicinity of magnetic phase transitions disorder fluctuations induce rare regions with an enhanced local critical temperature. These large clusters are ordered on the scale of the correlation length and act as effective spins. Though rare in occurrence they carry a considerable amount of magnetic entropy and the overall effect is the appearance of singular, thermodynamic responses. This magnetic Griffiths phase picture has been advocated as a source of NFL behavior in disordered heavy fermion systems.[37] However, very recent results seem to point to several difficulties encountered when this scenario is applied to experimental systems, as follows.

The entropy problem. The amount of magnetic entropy observed experimentally in most disordered heavy fermion systems seems much too high to be compatible with the magnetic Griffiths phase picture. Taking the measured specific heat of, say, $UCu_{5-x}Pd_x$, we estimate that about 5% of the sample would have to participate in the spin-$\frac{1}{2}$ clusters. This implies an average cluster separation of 2-3 lattice constants, ruling out cluster sizes exceeding this distance. These small clusters suggest instead that the ''unquenched'' localized moments of the KDM/DMFT or the electronic Griffiths phase offer a much more natural explanation.

Effects of dissipation. Other important limitations of the magnetic Griffiths phase scheme have also been emphasized in recent work by Millis, Morr, and Schmalian,[39] who have carefully examined the effects of dissipation caused by the metallic bath. This work suggests that the dissipation caused by itinerant electrons is so pronounced that quantum tunneling of even moderately sized magnetic clusters will be suppressed. Although the emergence of a magnetic Griffiths phase is a well established phenomenon in disordered *insulating* magnets, this result seems to bring into question its relevance to itinerant systems.

(3) *Spin glass precursors.* Finally, another possibility is to invoke the proximity to a spin glass quantum phase transition. Several theoretical schemes predicting non-Fermi liquid behavior in the vicinity of a spin-glass quantum critical point have been proposed.[40–42] Spin glass phases have been identified in the phase diagram of some heavy fermion alloys ($UCu_{5-x}Pd_x$, for $x>1.5$)[43] and structurally disordered compounds (URh_2Ge_2).[44] More interestingly, evidence of glassy dynamics *in the absence of freezing* at very low temperatures has been seen in $UCu_{5-x}Pd_x (x=1,1.5)$[45] and $Ce(Ru_{0.5}Rh_{0.5})_2Si_2$,[15,46] with conflicting results pointing to a very low freezing temperature in $UCu_{3.5}Pd_{1.5}$.[43] These experiments seem to suggest that, if there is a true spin glass transition, freezing temperatures are *strongly suppressed* in a wide portion of the phase diagram.

II. THE MODEL AND ITS SOLUTION

A. The statistical dynamical mean-field theory

A simplified Hamiltonian capable of capturing the essential physics of disordered metals with localized moments is provided by a disordered Anderson lattice

$$H = H_c + H_f + H_{\rm hyb}, \tag{1}$$

where

$$H_c = -t \sum_{\langle ij\rangle\sigma} (c^\dagger_{i\sigma} c_{j\sigma} + \text{H.c.}) + \sum_{j\sigma} (\epsilon_j - \mu) c^\dagger_{j\sigma} c_{j\sigma}, \tag{2}$$

$$H_f = \sum_{j\sigma} E_f f^\dagger_{j\sigma} f_{j\sigma} + U \sum_j f^\dagger_{j\uparrow} f_{j\uparrow} f^\dagger_{j\downarrow} f_{j\downarrow}, \tag{3}$$

$$H_{\rm hyb} = \sum_{j\sigma} (V_j f^\dagger_{j\sigma} c_{j\sigma} + \text{H.c.}). \tag{4}$$

In Eqs. (2)–(4), $c_{j\sigma}$ ($f_{j\sigma}$) annihilates a conduction (f) electron on site j with spin projection σ, t is the nearest neighbor hopping amplitude, μ is the chemical potential, U is the f-site Coulomb repulsion, E_f is the f-energy level, and we introduce random conduction electron on-site energies (ϵ_j) and hybridization matrix elements V_j. These are chosen from given distributions $P_1(\epsilon)$ and $P_2(V)$, taken to be either square or Gaussian, with width and standard deviation W, respectively. We have also studied discrete cases of $P_2(V)$. There is a large degree of uncertainty as to a realistic model of disorder for heavy fermion alloys. A rather thorough study of the local f-site environment in the alloys $UCu_{5-x}Pd_x$ ($x=1$ and 0.5) was carried out in Refs. 32,33 through XAFS experiments. These authors were able to determine the amount of Pd/Cu site interchange as well as the U-Cu bond length distributions. In order to accommodate both types of fluctuations one must, in principle, allow for a distribution of both hybridization strengths *and* on-site conduction electron energies. On the other hand, when the local moments are randomly replaced by non-magnetic elements (the so-called ''Kondo holes''), spatial fluctuations of E_f should also be included.[17] Throughout the paper, we use the half bandwidth D as energy unit. For the Bethe lattice (to be introduced later), $D=2\sqrt{2}t$ if the coordination number is 3. This should be contrasted to Ref. 18, where W is measured in units of t. Note also that the f-level energy E_f is always measured *relative to the chemical potential*. This is to ensure that, by making it negative and large enough in absolute value, we always work in the local moment/Kondo regime.

We worked within the framework of the statDMFT.[34,35] This treatment is able to incorporate both strong local correlations and Anderson localization effects in a fully self-consistent fashion. Although the method has been described before in the context of the disordered Hubbard model,[35] we will briefly review it with the dual goal of setting the nota-

tion and extending it to the disordered Anderson lattice. It starts by focusing on a generic unit cell j of the lattice, containing an f site and its adjoining conduction electron Wannier state, and writing its effective action in imaginary time as

$$S_{\text{eff}}(j) = S_c(j) + S_f(j) + S_{\text{hyb}}(j), \tag{5}$$

$$S_c(j) = \sum_\sigma \int_0^\beta d\tau \int_0^\beta d\tau' c^\dagger_{j\sigma}(\tau)[\delta(\tau-\tau')(\partial_\tau + \epsilon_j - \mu) + \Delta_{cj}(\tau-\tau')]c_{j\sigma}(\tau'), \tag{6}$$

$$S_f(j) = \int_0^\beta d\tau \Big[\sum_\sigma (\partial_\tau + E_f) f^\dagger_{j\sigma}(\tau) f_{j\sigma}(\tau) + U n_{fj\uparrow}(\tau) n_{fj\downarrow}(\tau) \Big], \tag{7}$$

$$S_{\text{hyb}}(j) = \sum_\sigma \int_0^\beta d\tau [V_j f^\dagger_{j\sigma}(\tau) c_{j\sigma}(\tau) + \text{H.c.}], \tag{8}$$

where $n_{fj\sigma} = f^\dagger_{j\sigma} f_{j\sigma}$. In writing Eqs. (5)–(8), a simplification has been made of retaining only quadratic contributions in fermionic fields after integrating out the other sites (in addition to the instantaneous Hubbard term), very similar to the usual dynamical mean-field theory.[24] The bath (or "cavity") function $\Delta_{cj}(\tau)$ in Eq. (6) is given by

$$\Delta_{cj}(\tau) = t^2 \sum_{l,m=1}^{z} G^{(j)}_{clm}(\tau), \tag{9}$$

where the sum extends over the z nearest neighbors and

$$G^{(j)}_{clm}(\tau) = -\langle T[c_{m\sigma}(\tau) c^\dagger_{l\sigma}(0)]\rangle^{(j)}$$

is the Green's function for propagation from nearest-neighbor site l to nearest-neighbor site m, calculated with the site j removed. Integrating out the remaining conduction electron $c_{j\sigma}$, we get the effective action of an auxiliary single-impurity Anderson model at each site j

$$S_{\text{imp}}(j) = \sum_\sigma \int_0^\beta d\tau \int_0^\beta d\tau' f^\dagger_{j\sigma}(\tau)[\delta(\tau-\tau')(\delta_\tau + E_f) + \Delta_{fj}(\tau-\tau')]f_{j\sigma}(\tau') + \int_0^\beta d\tau U n_{fj\uparrow}(\tau) n_{fj\downarrow}(\tau), \tag{10}$$

where the hybridization function for the f site is, in Matsubara frequency space,

$$\Delta_{fj}(i\omega_n) = \frac{V_j^2}{i\omega_n - \epsilon_j + \mu - \Delta_{cj}(i\omega_n)}. \tag{11}$$

The solution of this impurity problem is the major difficulty in this treatment. We implemented two different methods of solution, which will be expanded upon in the next subsections. The aim is to calculate the local f-electron Green's function

$$G^{\text{loc}}_{fj}(\tau) = -\langle T[f_{j\sigma}(\tau) f^\dagger_{j\sigma}(0)]\rangle, \tag{12}$$

under the dynamics dictated by Eq. (10). It is conveniently parametrized by its self-energy

$$G^{\text{loc}}_{fj}(i\omega_n) = \frac{1}{i\omega_n - E_f - \Delta_{fj}(i\omega_n) - \Sigma_{fj}(i\omega_n)}. \tag{13}$$

It is also convenient to define a local conduction electron Green's function

$$G^{\text{loc}}_{cj}(\tau) = -\langle T[c_{j\sigma}(\tau) c^\dagger_{j\sigma}(0)]\rangle, \tag{14}$$

such that

$$G^{\text{loc}}_{cj}(i\omega_n) = \frac{1}{i\omega_n - \epsilon_j + \mu - \Delta_{cj}(i\omega_n) - \Phi_j(i\omega_n)}, \tag{15}$$

where

$$\Phi_j(i\omega_n) = \frac{V_j^2}{i\omega_n - E_f - \Sigma_{fj}(i\omega_n)}. \tag{16}$$

We note that the $\Phi_j(i\omega_n)$ function describes the local scattering of the conduction electrons off the f shell at site j, incorporating information about both elastic and inelastic processes.

All the information a generic site j has about the rest of the lattice is encoded in the bath function (9), which should be viewed as a functional of the conduction electron lattice Green's function. Since a fully analytical treatment is impossible, we have to solve the equations numerically. For this purpose, we formulated the problem on a Bethe lattice, where things are considerably simplified as explained in Ref. 35. In this case, nearest neighbors l and m become disconnected once j is removed and only local Green's functions survive

$$G^{(j)}_{clm}(i\omega_n) = \delta_{l,m} G^{(j)}_{cll}(i\omega_n) = \delta_{l,m} G^{\text{loc}(j)}_{cl}(i\omega_n).$$

Finally, these last objects can be computed from an action at site l in almost all aspects identical to Eqs. (5)–(8), the only difference now being that the bath function sum runs over the $z-1$ nearest neighbors (here labeled by m) only

$$\Delta^{(j)}_{cl}(i\omega_n) = t^2 \sum_{m=1}^{z-1} G^{\text{loc}(l)}_{cm}(i\omega_n). \tag{17}$$

Note that, on the right-hand side, we do not need to specify that site j has been excluded as the removal of l completely disconnects sites labeled by m from site j (this property is specific to the Bethe lattice). The reappearance of $G^{\text{loc}}_{cm}(l)(i\omega_n)$, whose distribution is identical to that of $G^{\text{loc}}_{cl}(j)(i\omega_n)$ since all sites are equivalent, closes the loop and establishes a recursive set of stochastic equations. When the interaction is turned off ($U=0$), this treatment reduces to the well-known self-consistent theory of localization,[47] here generalized to a two-band lattice. When we take the coordination to infinity $z\to\infty$ keeping $\tilde{t} = t/\sqrt{z} = \text{const}$, our treatment reduces to the DMFT of correlations and

disorder.[16,17,24] In the latter case, the disorder treatment is equivalent to the CPA,[25] which has no localization transition.

A full solution of Eqs. (5)–(17) for given distributions $P_1(\epsilon)$ and/or $P_2(V)$ involves solving an ensemble of impurity problems self-consistently. Physically, the conduction electrons propagate through a disordered lattice and scatter off conduction site potential fluctuations as well as *f*-site resonances. These resonances, in turn, describe the formation of localized moments, whose local Kondo temperatures fluctuate as well, reflecting a disordered conduction sea environment. Complete statistical information can in principle be obtained from the distributions of the various renormalized local quantities. We stress that a random distribution of any bare parameter causes all renormalized quantities to fluctuate as a result of the self-consistent nature of our treatment. Therefore, even if we include only fluctuations in the conduction sea through $P_1(\epsilon)$, *a distribution of Kondo temperatures ensues*.[31,48] This is easily seen from the approximate formula for the Kondo temperature in the Kondo limit $(\Sigma_\sigma n_{fj\sigma} \approx 1)$[49]

$$T_K \approx D \exp\left(-\frac{1}{\rho_j J_j}\right), \tag{18}$$

where ρ_j is the local density of states (DOS) seen by the *f* site

$$\rho_j \approx \frac{\mathrm{Im}[\Delta_{fj}(0-i\eta)]}{\pi V_j^2} \tag{19}$$

and J_j is the Kondo coupling constant, given in the Kondo limit by

$$J_j \approx 2V_j^2\left(\frac{1}{|E_f|}+\frac{1}{|E_f+U|}\right). \tag{20}$$

Even if V_j is not random, the local DOS is, because of the denominator in Eq. (11). As a result of the strong exponential dependence in (18), even mild localization effects can be strongly enhanced and should be seriously considered, specially in disordered heavy fermion systems.

B. The impurity solvers

An important part of the method we employed is the solution of the impurity problems posed by the ensemble of effective actions given by Eq. (10) and its counterpart for a site with one nearest neighbor removed. We concentrated mostly on two methods of solution, which we now briefly describe: the slave boson, large-*N* based, mean-field theory, and second-order perturbation theory in *U*. In order to unclutter the notation, we drop in the next subsections the site index *j* and the superscript loc. Details of the numerical treatment are given in the Appendix.

1. Slave boson mean-field theory

This method gives a good description of the low temperature, Fermi liquid regime of the Anderson impurity problem in the limit $U \to \infty$ and is extensively covered in the literature.[21,22] Its main advantage is the ability to capture the zero temperature fixed point correctly as well as the exponential nature of the low energy scale. Its treatment of the self-energy, however, does not incorporate inelastic processes to leading order. In addition, it has a spurious phase transition at a finite temperature, where in reality there should be only a smooth crossover. For these reasons, we confine it to the zero temperature limit, where it is a useful guide. As applied to our problem, the method has been described in Appendix D of Ref. 17 and we will merely state the results, generalized to the Matsubara frequency axis and at $T=0$. The local *f*-electron Green's function is given by

$$G_f(i\omega) = \frac{q}{i\omega - \epsilon_f - q\Delta_f(i\omega)} \tag{21}$$

$$\equiv q G_f^{\mathrm{qp}}(i\omega), \tag{22}$$

where the last equality defines the local *f*-electron *quasi particle* Green's function and the variational parameters ϵ_f (renormalized *f* energy) and q (quasiparticle residue) are determined from the solution of the set of equations

$$\epsilon_f - E_f + \int_{-\infty}^{\infty} \frac{d\omega}{\pi} \Delta_f(i\omega) G_f^{\mathrm{qp}}(i\omega) = 0, \tag{23}$$

$$q + \int_{-\infty}^{\infty} \frac{d\omega}{\pi} e^{i\omega\eta} G_f^{\mathrm{qp}}(i\omega) = 1. \tag{24}$$

Using

$$\int_{-\infty}^{\infty} \frac{d\omega}{\pi} e^{i\omega\eta} \mathrm{Im}[G_f^{\mathrm{qp}}(i\omega)] = 1,$$

Eqs. (23)–(24) simplify to

$$2\int_0^{\infty} \frac{d\omega}{\pi} \mathrm{Re}[\Delta_f(i\omega) G_f^{\mathrm{qp}}(i\omega)] = E_f - \epsilon_f, \tag{25}$$

$$q + 2\int_0^{\infty} \frac{d\omega}{\pi} \mathrm{Re}[G_f^{\mathrm{qp}}(i\omega)] = 0. \tag{26}$$

Equation (16) becomes in this approximation

$$\Phi(i\omega) = \frac{qV^2}{i\omega - \epsilon_f}. \tag{27}$$

2. Second-order perturbation theory

The perturbative solution of the single-impurity Anderson model with particle-hole symmetry was thoroughly analyzed by Yamada and Yosida.[50–53] The series expansion in *U* for physical quantities such as the specific heat and the spin susceptibility converges very fast and even second-order results can be useful.[54] Extension of the perturbative treatment to the case without particle-hole symmetry poses considerable difficulties. A particularly useful proposal is the use of an interpolative self-energy which recovers the atomic ($V \to 0$) and high frequency limits.[55] Further improvements of the method were later suggested.[56,57]

The procedure consists in defining an unperturbed *f*-electron Green's function

$$G_f^{(0)}(i\omega_n) = \frac{1}{i\omega_n + \tilde{\mu} - \Delta_f(i\omega_n)}, \tag{28}$$

with a new parameter $\tilde{\mu}$ to be determined later, which vanishes at particle-hole symmetry. The interacting Green's function is given in Eq. (13). The interpolative self-energy is[56,57]

$$\Sigma_f(i\omega_n) = Un + \frac{A\Sigma^{(2)}(i\omega_n)}{1 - B\Sigma^{(2)}(i\omega_n)}, \tag{29}$$

where

$$n = T\sum_{\omega_n} e^{i\omega_n\eta} G_f(i\omega_n) \tag{30}$$

and

$$\Sigma^{(2)}(i\omega_n) = -U^2 \int_0^\beta d\tau e^{i\omega_n\tau} [G_f^{(0)}(\tau)]^2 G_f^{(0)}(-\tau). \tag{31}$$

The last equation (31) is the usual second order diagram using the unperturbed Green's function (28) for the internal lines. The parameters A and B are determined by imposing the high frequency and atomic limits, respectively, and are given by[56]

$$A = \frac{n(1-n)}{n_0(1-n_0)}, \tag{32}$$

$$B = \frac{(1-n)U + E_f + \tilde{\mu}}{n_0(1-n_0)U^2}, \tag{33}$$

where

$$n_0 = T\sum_{\omega_n} e^{i\omega_n\eta} G_f^{(0)}(i\omega_n). \tag{34}$$

Different schemes have been proposed in order to fix the free parameter $\tilde{\mu}$.[55–57] At zero temperature, one can ensure that the low energy Fermi liquid behavior is obtained by imposing the Friedel sum rule.[56] This procedure cannot be easily generalized to finite temperatures, however. One option is to fix $\tilde{\mu}$ at its zero temperature value even at finite temperatures. Alternatively, one can require at any temperature[55]

$$n = n_0, \tag{35}$$

which makes $A=1$. Finally, a third possibility is imposing $\tilde{\mu}=\mu$.[57] These three alternatives have been rather carefully compared in Ref. 57 at $T=0$ and checked against exact diagonalization. The first two methods were shown to be almost equivalent whereas the third one is inferior. Moreover, comparisons at finite temperatures with Quantum Monte Carlo results confirmed the adequacy of imposing Eq. (35).[58] Specific applications to a clean Anderson lattice model further corroborated this conclusion.[59,60] Thus, our results were based on imposing condition (35). It should be remembered, however, that the perturbative solution predicts a characteristic energy scale that is *quantitatively* incorrect at large values of U, since it is unable to capture the correct exponential dependence. Nevertheless, for moderate interactions, it still gives reasonable results. Within its limitations, this perturbative scheme is a relatively flexible low-cost tool to tackle the impurity problem with the great advantage of being able to naturally account for *inelastic* processes.

We note that a direct comparison between the slave boson mean field theory results and second order perturbation theory is not possible because the former is limited to the $U\to\infty$ limit, which is obviously outside the region of validity of the latter. The main interest of an analysis of both methods, however, resides in the exploration of *the importance of inelastic processes*, which are absent in the slave boson mean-field treatment.

III. SLAVE BOSON MEAN-FIELD THEORY RESULTS

We now present the results obtained at $T=0$ using the slave boson mean-field theory as an impurity solver. Most of our results were obtained for a uniform distribution of on-site conduction electron energies

$$P_1(\epsilon) = \frac{1}{W}; \quad |\epsilon| \leqslant \frac{W}{2}.$$

In Sec. III C we also show results for a discrete distribution of hybridization strengths $P_2(V)$.

A. Conduction electron typical density of states

To understand the overall behavior as a function of disorder, it is instructive to consider the transport properties of the conduction electrons. Since there are no interactions among them in our model, their behavior is that of a disordered noninteracting electron system. There are two sources of disorder, as can be seen in Eq. (15): fluctuations of the local on-site energies ϵ_j and of the f-shell resonances described by $\Phi_j(i\omega_n)$. They are not independent, however, since they are inextricably tied by self-consistency. Their combined effect acts to decrease the conduction electron mobility.

1. Typical density of states: an order parameter for localization

A useful measure of this mobility is given by the *typical* value of the local escape rate. This is encoded in the imaginary part of the local conduction electron Green's function (the local DOS) at zero frequency $\rho_{cj} = (1/\pi)\mathrm{Im}[G_{cj}^{\mathrm{loc}}(0 - i\delta)]$. We will, from now on, drop the superscript denoting the removal of a nearest neighbor so as to lighten the notation. As shown originally by Anderson, the typical value of the local DOS vanishes when the electrons are localized and can be viewed as an order parameter for the localization transition.[61] A convenient way of accessing the typical value is furnished by the geometric average

$$\rho_c^{\mathrm{typ}} = \exp\{\overline{\ln \rho_{cj}}\}, \tag{36}$$

where the overbar denotes a disorder average. By contrast, the arithmetic average

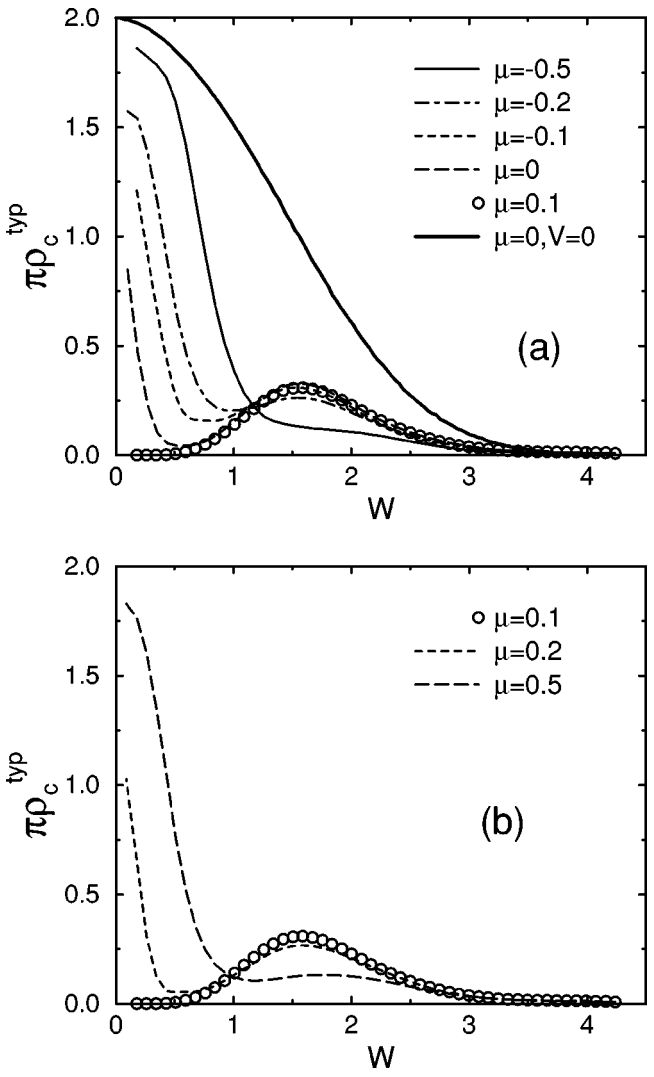

FIG. 1. Typical conduction electron density of states as a function of disorder strength for several values of the chemical potential μ, using slave boson mean field theory as the impurity solver. We used $E_f=-1$, $V=0.5$, except for the thick solid line in (a), which is for $V=0$.

$$\rho_c^{\mathrm{av}}=\overline{\rho_{cj}} \tag{37}$$

is finite at the transition. A thorough analysis of the critical behavior of the local DOS distribution in the noninteracting Bethe lattice localization problem was carried out in Ref. 62. In Fig. 1 we show the typical conduction electron DOS as a function of disorder for several values of the chemical potential.

2. Proximity to the Kondo insulator

We can identify three qualitatively distinct behaviors.[19] For $\mu\lesssim -0.4$ and for $\mu\gtrsim 0.5$, ρ_c^{typ} is a monotonically decreasing function of disorder. For $\mu\approx 0.1$, the clean system is a Kondo insulator[63,64] and $\rho_c^{\mathrm{av}}=\rho_c^{\mathrm{typ}}=0$. As disorder is introduced in the Kondo insulator, ρ_c^{typ} initially increases, reaching a maximum at about $W\approx 1.5$, after which it decreases monotonically. Finally, for $-0.3\lesssim\mu\lesssim 0.1$ and $0.1\lesssim\mu\lesssim 0.4$ ρ_c^{typ} initially decreases, passes through a minimum around $W\approx 0.5-1$, then increases up to a maximum at about $W\approx 1.5$ and eventually becomes monotonically decreasing. For all values of μ, the typical DOS vanishes at a disorder-induced metal insulator transition (MIT) at $W_{\mathrm{MIT}}\approx 4.5$.

These distinct behaviors can be traced back to how close the clean system is to the Kondo insulator point[63,64] at $\mu\approx 0.1$.[19] If we start from the clean insulator, the introduction of disorder acts to create states inside the gap, thus increasing the DOS at the chemical potential. This increase continues until the gap is essentially washed out and the system becomes a bad metal. After that, localization intervenes and ρ_c^{typ} starts to decrease towards the MIT.

For fillings close to but not at the Kondo insulator point, the clean system is a heavy fermion metal at $T=0$. The f resonances $[\Phi(\omega)]$ coherently scatter the conduction electrons creating a strongly renormalized Fermi liquid. In the slave boson treatment, $\Phi(\omega)$ diverges at $\omega=\epsilon_f$, see Eq. (27), corresponding to the limit of unitary scattering, with a maximally allowed phase shift $\delta=\pi/2$. We can view its value at the Fermi level $\Phi(0)=-qV^2/\epsilon_f$ (which is real at $T=0$) as an effective potential coming from the f electrons. The closer the system is to the Kondo insulator, the larger the value of $\Phi(0)$, the insulator being signaled by the divergence of this quantity (or equivalently by $\epsilon_f=0$). The effect of disorder is to immediately start generating spatial fluctuations of the f resonances, with different phase shift values at the chemical potential. Proximity to the insulator implies large, random, almost unitary scattering potentials. As a result, metallic coherence is efficiently destroyed and the typical conduction electron DOS is strongly suppressed.[18,19] The important role played by the unitary scatterers was emphasized in Refs. 19 and 18, where the distribution $P\{1/[\Phi(0)]\}$ was directly computed and its weight at $1/\Phi(0)=0$ was shown to correlate with the destruction of coherence.

There is another equivalent way of understanding these effects. For small dopings away from the Kondo insulator, carriers are introduced at the *edges* of the valence or conduction bands defined by the Kondo insulator gap, which have a small DOS (in the Bethe lattice, band edges have a square root shape as in three dimensions). As has been known for a long time, a region of small DOS is particularly sensitive to localization effects introduced by disorder.

As in the previous case, further increase of disorder acts to wash out the nearby Kondo pseudogap and the behavior then becomes very similar to the disordered Kondo insulator. We thus have a region with a rather nonintuitive increasing ρ_c^{typ}, which can be ascribed to the proximity to the Kondo insulator fixed point. The behavior at fillings well away from the Kondo insulator is much less influenced by the pseudogap, see Fig. 1 for $\mu=\pm 0.5$. Although there is a rapid initial decrease of ρ_c^{typ}, followed by a much slower dependence, the typical DOS does not exhibit the unconventional increase with disorder observed at other fillings.

3. Role of the hybridization strength

It is interesting to note that the critical value of disorder for the MIT W_{MIT} depends on the hybridization strength. In

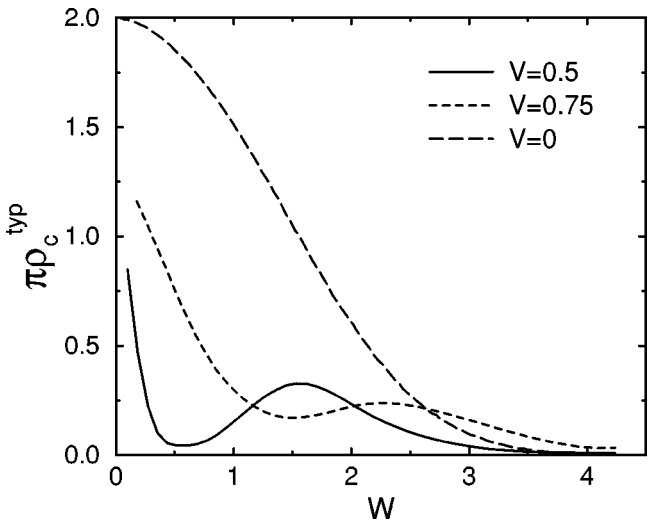

FIG. 2. Typical conduction electron density of states as a function of disorder strength for different values of hybridization V, using slave boson mean field theory as the impurity solver ($E_f=-1$ and $\mu=0$).

Fig. 2, we show the disorder dependence of the typical conduction electron DOS for different values of V. There is hardly any change in W_{MIT} as we go from $V=0$ to $V=0.5$ (see also Fig. 1). However, for $V=0.75$, the critical disorder strength is clearly enhanced. This figure also illustrates the nontrivial nature of the self-consistency. Indeed, the two types of disorder coming from fluctuations in ϵ_j and Φ_j are clearly not independent, since the *addition* of f-site disorder as we turn on V from 0 to 0.75 acts to *increase* the mobility for $W \gtrsim 2.8$. The self-consistently determined solutions of the impurity problems effectively help *screen* the conduction electron disorder. Note also how an increased value of V pushes the ''dip-hump'' structure to higher values of disorder. Since the Kondo insulating gap increases with the hybridization strength, this is consistent with our explanation for the nature of this nonmonotonic behavior.

B. Distribution of the conduction electron local density of states

One of the great advantages of the present approach is the possibility of monitoring complete distribution functions. Many of the features exhibited in Figs. 1 and 2 can be directly read off the distribution of $\pi\rho_c=\mathrm{Im}[G_c^{\mathrm{loc}}(0-i\delta)]$. We show this by plotting $P\{\log_{10}\mathrm{Im}[G_c^{\mathrm{loc}}(0-i\delta)]\}$ for several disorder strengths and different chemical potential values in Fig. 3. It follows from the definition of $\pi\rho_c^{\mathrm{typ}}$, Eq. (36), that it is obtained by raising 10 to the power of the average of this distribution (we use powers of 10 for ease of computation). For weak disorder in the metallic cases [Figs. 3(a) and (b), $P\{\log_{10}\mathrm{Im}[G_c^{\mathrm{loc}}(0-i\delta)]\}$ is approximately Gaussian, *even though the bare disorder is uniform*, a feature shared by several physical quantities.[18,19] This is due to the presence of correlations between many distant lattice sites mediated by the extended conduction electron wave function, which introduces a sort of averaging effect. In the

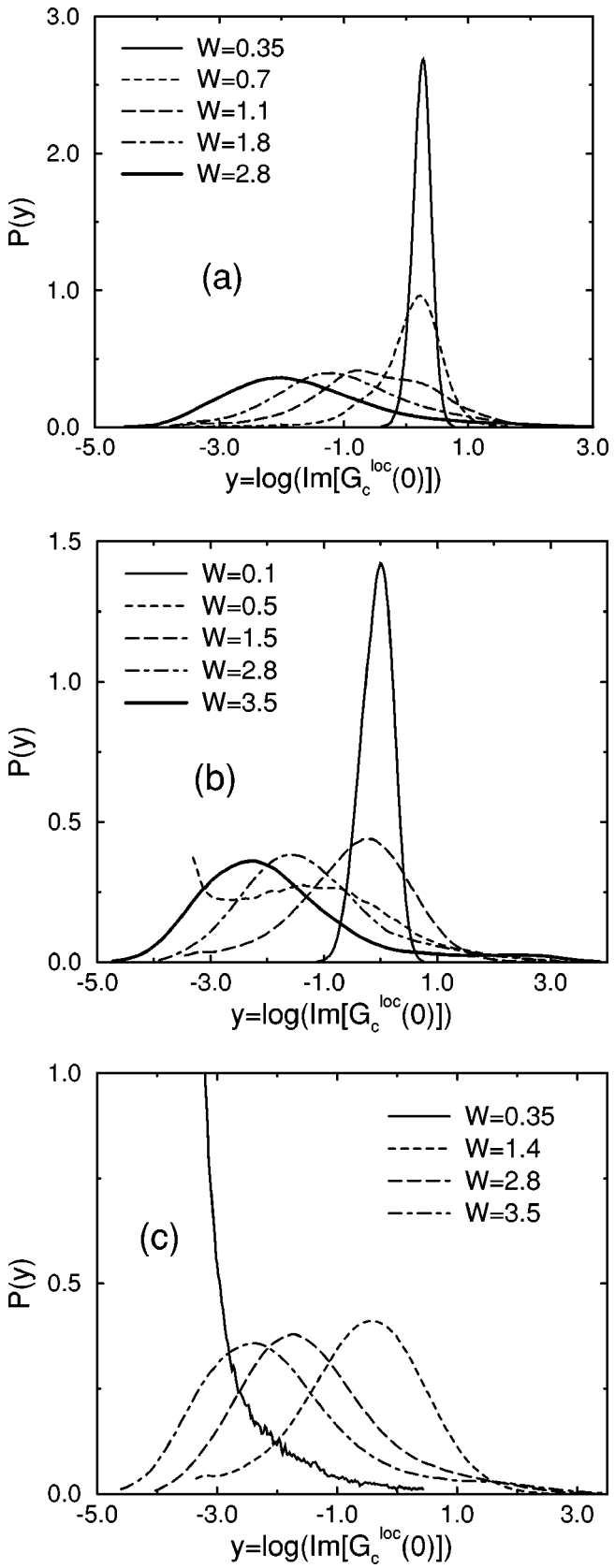

FIG. 3. Distributions of the logarithm of $\mathrm{Im}[G_c^{\mathrm{loc}}(0-i\delta)]$ for several values of disorder strength, using slave boson mean field theory as the impurity solver: (a) $\mu=-0.5$, (b) $\mu=0$, and (c) $\mu=0.1$ ($V=0.5$, $E_f=-1$).

Kondo insulator case [Fig. 3(c)], however, the distribution is *not* Gaussian at weak disorder. Keeping in mind that $\rho_c = 0\{\log_{10} \mathrm{Im}[G_c^{\mathrm{loc}}(0 - i\delta)] \to -\infty\}$ in the clean Kondo insulator, it is clear that the introduction of weak disorder has to generate weight at very small $\pi\rho_c$. Indeed, $P\{\log_{10} \mathrm{Im}[G_c^{\mathrm{loc}}(0 - i\delta)]\}$ shows a divergence at $\mathrm{Im}[G_c^{\mathrm{loc}}(0 - i\delta)] \approx 10^{-3}$ for $W = 0.35$. For large values of W the distribution becomes extremely broad, spanning many orders of magnitude. In the case $\mu = -0.5$ [Fig. 3(a)], corresponding to a system well away from the Kondo insulator filling, the distribution broadens and its maximum steadily shifts towards lower values as disorder is increased. This is to be expected from the monotonic behavior of ρ_c^{typ}. Likewise, at $\mu = 0$, the nonmonotonic behavior of the typical value is also clearly reflected in $P\{\log_{10} \mathrm{Im}[G_c^{\mathrm{loc}}(0 - i\delta)]\}$ [see Fig. 3(b) and compare it to Fig. 1(a)].

As we saw, at the Kondo insulating chemical potential $\mu = 0.1$ and for $W = 0.35$, the distribution shows a divergence at $\mathrm{Im}[G_c^{\mathrm{loc}}(0 - i\delta)] \approx 10^{-3}$. A similar diverging *tendency* is observed at $\mu = 0$ [Fig. 3(b)] and $W = 0.5$. This is precisely the disorder value where the minimum of ρ_c^{typ} occurs [see Fig. 1(a)] and which we have been ascribing to the presence of many unitary scatterers due to the nearby Kondo insulator. The similarity between the two distributions strengthens further our case for the importance of the proximity to the Kondo insulator. Additionally and consistent with this, the divergence is totally absent at $\mu = -0.5$, where the role played by the Kondo insulator fixed point is much less important.

It is also interesting to observe in Fig. 3(c), how the Kondo gap is washed out by disorder: at $W = 1.4$, where ρ_c^{typ} peaks [Fig. 1(a)], most of the weight of the distribution is already at sizeable values of the DOS and its shape is very similar to the metallic cases.

C. Distribution of Kondo temperatures

We now proceed to the analysis of the physical properties related to the ensemble of impurity problems. As shown before[18,19] the distribution of Kondo temperatures of the various f sites is log normal for weak disorder, but broadens and acquires a power law shape at intermediate values of $W \approx 0.35 - 0.7$. Once this power law becomes singular enough, a Griffiths phase is entered with diverging thermodynamic responses.[18,19]

1. Universality at weak disorder

We have noticed that for weak disorder, the shape of the distribution of various quantities, including the Kondo temperature, is universal, irrespective of the shape of the bare distribution of disorder. A nice illustration of this effect is given by the case where the bare disorder is a *discrete* distribution. As an example, we take the discrete distribution of hybridization strengths $P_2(V)$, determined in Ref. 32 from XAFS measurements in $UCu_{5-x}Pd_x$. The resulting distribution of $\log_{10} T_K$ is shown in Fig. 4(a). It is continuous and has a log-normal shape. In Fig. 4(b) we show the distribution of T_K (smooth dot-dashed line) and compare it to the discrete distribution obtained in the DMFT (vertical solid lines),

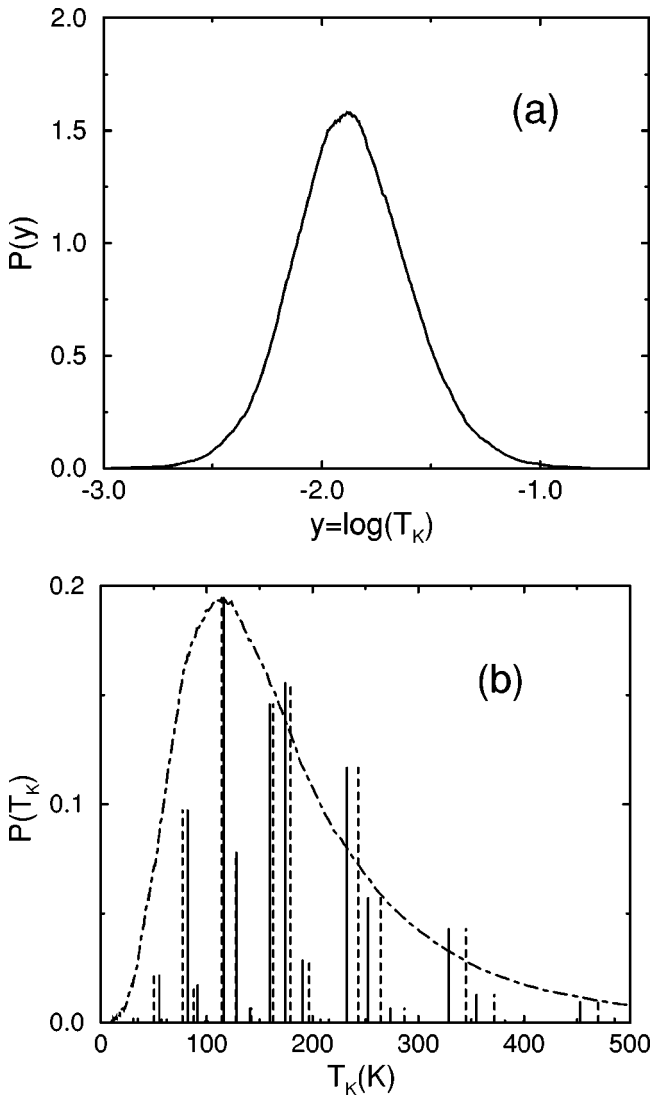

FIG. 4. (a) Distribution of the logarithm of the Kondo temperature for a discrete bare distribution of hybridizations, taken from Ref. 32, using slave boson mean field theory as the impurity solver (here, we use $t = 0.5$, $E_f = -5.54$, and $\mu = -0.2$), (b) Comparison between the smooth distribution of Kondo temperatures (dot-dashed line) obtained in the statDMFT and the discrete results of DMFT (vertical solid lines) and the Kondo disorder model (vertical dashed lines).

which corresponds to the limit of infinite coordination. We also include in the figure the results of the Kondo disorder model[13,32] (KDM) (vertical dashed lines), which is very similar to the DMFT. The only differences between the KDM and the DMFT are that, in the former, no self-consistency is imposed and a Kondo instead of an Anderson lattice model is used. The difference between the results of the KDM/DMFT and the statDMFT is striking. The fluctuations of the conduction electron wave functions incorporated in the statDMFT smooth out the discrete results of the DMFT into a universal continuous form. A description of the NFL behavior within the KDM/DMFT theory would be clearly impossible. This comparison also shows that this level of hybridization disorder alone is not able to generate non-Fermi-liquid behavior

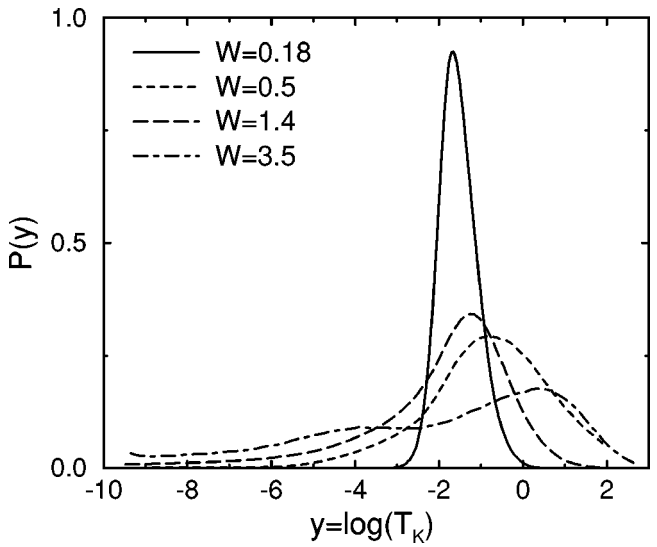

FIG. 5. Distribution of the logarithm of the Kondo temperature for different values of disorder, using slave boson mean field theory as the impurity solver ($V=0.5$, $E_f=-1$, and $\mu=0.2$).

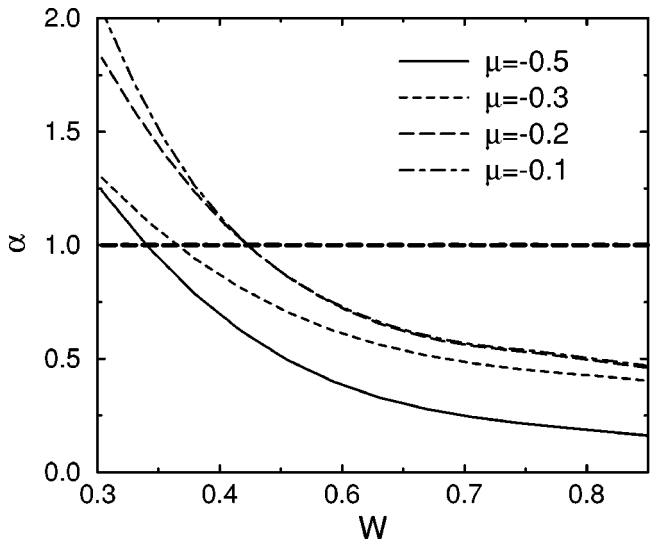

FIG. 6. Exponent of the power-law distribution of Kondo temperatures as a function of disorder for different values of the chemical potential ($V=0.5$, $E_f=-1$). The horizontal dashed line indicates the critical value for the emergence of NFL behavior, where $P(T_K)\propto$const and $\chi(T)\propto C(T)/T\propto\ln(T_0/T)$.

even in statDMFT, since the distribution of Kondo temperatures goes to zero as $T_K\to 0$, a point that was stressed in Refs. 32,33. However, if disorder in the conduction electron sites, $P_1(\epsilon)$ is also included a singular behavior can be obtained (not shown). The inclusion of conduction electron disorder is reasonable in $UCu_{5-x}Pd_x$, since the Cu-Pd interchange affects both V_j and ϵ_j.

2. Emergence of the electronic Griffiths phase

In order to identify the emergence of the Griffiths phase, we next study the evolution of the distribution of Kondo temperatures as the width W of $P_1(\epsilon)$ is varied (with no disorder in V). Typical results are shown in Fig. 5, corresponding to $\mu=0.2$. As the disorder increases, we find that the overall width, but most significantly, the size of the low-T_K tail rapidly grows. These tails assume a *power-law* form $P(T_K)\sim T_K^{\alpha-1}$, with the power $\alpha(W)$ being a monotonically decreasing function of disorder. Once again, this behavior cannot be obtained in the rigid scheme of the KDM/DMFT without unjustified fine tuning. The thermodynamic response of the system assumes a singular, non-Fermi liquid form as soon as $\alpha\leqslant 1$, which happens for sufficiently strong disorder $W\geqslant W_{\rm NFL}\approx 0.35-0.45$. Since this behavior does not reflect any thermodynamic phase transition, it assumes the character of an electronic Griffiths phase. Here, singular behavior emerges due to the presence of exponentially rare events (in our case Kondo spins) which nevertheless provide an exponentially large contribution to thermodynamic and transport properties and thus dominate the macroscopic behavior of the system. The W dependence of the exponent α can be easily obtained by fitting the tails of these distributions; a representative behavior for several values of the chemical potential is shown in Fig. 6.

3. NFL and the proximity to the Kondo insulator

In the previous section we have seen how the proximity of the Kondo insulator plays a crucial role in determining the disorder dependence of the localization and transport properties, and leads to the surprising ''bad metal'' behavior for a wide parameter range. This was argued to reflect the enhanced sensitivity to disorder of those electronic states that are very close to the Kondo insulator, and which are most easily affected by localization effects. We have also established that NFL behavior also emerges as a result of disorder-induced density of states fluctuations. It is then natural to ask how sensitive this emergence of NFL behavior is to the proximity to the Kondo insulator, which in the clean limit emerges only in a narrow parameter range, close (in our case) to $\mu\sim 0.1$.

To address this question, we have systematically investigated the evolution of $P(T_K)$ as a function of the distance to the Kondo insulator, i.e., as a function of the chemical potential μ. The behavior for weak disorder ($W=0.18$) is shown in Fig. 7. Despite what one would naively expect, these result clearly demonstrate that the distributions are the broadest *far* from the Kondo insulator. As we can see on this figure, the distributions narrow down as the Kondo insulator is approached from either side. As a result, we may expect that the critical disorder strength $W_{\rm NFL}$ necessary for the emergence of NFL behavior should *increase* closer to the Kondo insulator. This surprising result is confirmed by examining the μ dependence of the exponent α as shown in Fig. 6. As we can see there, for a given W, the exponent α is indeed *smaller*, and $W_{\rm NFL}$ decreases for larger μ (far from the Kondo insulator).

At first sight, these findings seem in contradiction to what one may expect, since we have found that the typical density of states decreases close to the Kondo insulator. Naively, one could then expect the Kondo temperatures to be depressed as well, leading to broader distributions and enhanced NFL behavior. On the other hand, we know that the Kondo temperature remains *finite* within the Kondo insulator, despite the

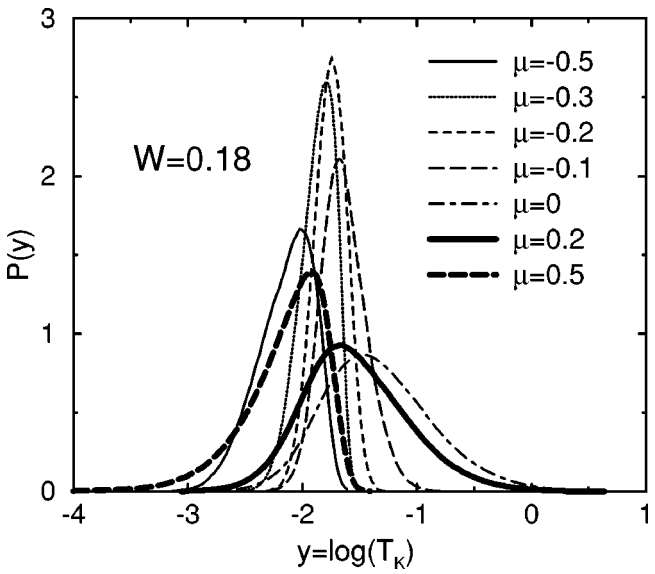

FIG. 7. Distribution of the logarithm of the Kondo temperature for different values of the chemical potential and fixed disorder $W=0.18$, using slave boson mean field theory as the impurity solver ($V=0.5$, $E_f=-1$).

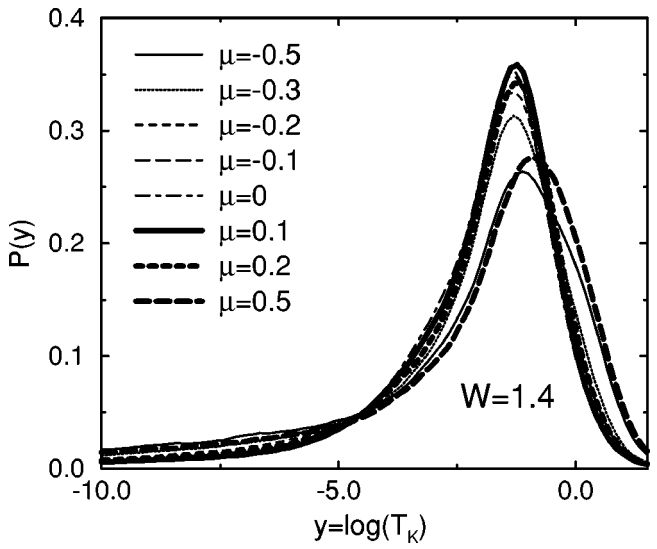

FIG. 8. Distribution of the logarithm of the Kondo temperature for different values of the chemical potential and fixed disorder $W=1.4$, using slave boson mean field theory as the impurity solver ($V=0.5$, $E_f=-1$).

fact that the density of states at the Fermi energy vanishes there. Although surprising at first sight, this curious feature of Kondo insulators is at present well understood. It is called the "strong coupling Kondo effect."[65–67] It reflects the fact that the Kondo screening is not determined only by electronic states precisely *at* the Fermi energy, but also by all the states in an energy interval of order T_K around the Fermi energy. Indeed, the average value of the Kondo temperature (see Fig. 7) is the *highest* precisely near the Kondo insulator. In the presence of disorder, the value of the Kondo temperature is determined by a certain weighted average of the density of states over this extended energy interval. When localization is present, only the states closest to the Kondo gap band edge will be appreciably affected, but since not only those states determine T_K, the net effect is washed away. We thus conclude that the proximity to the Kondo insulator, in contrast to transport, does not have appreciable effect on the emergence of the NFL behavior. Indeed, the critical value of disorder W_{NFL} required for the emergence of NFL behavior is found to have a remarkably weak μ dependence.

4. Universality at strong disorder

At strong disorder we expect the density of states fluctuations to completely wash out any trace of the Kondo gap and, in addition, to broaden the conduction band, making it very flat and featureless. As a result, all quantities are expected to have an extremely weak μ dependence, leading to a more universal behavior of all quantities. Such behavior is indeed seen at sufficiently strong disorder, where the typical DOS curves (Fig. 1) are seen to merge around $W\sim 1.4$. A similar behavior is seen in Fig. 8, which shows $P(\log_{10} T_K)$ for different μ's at $W=1.4$. This universal behavior is even more striking if this distribution is plotted on a log-log scale (Fig. 9), where an almost perfect power-law tail ($\alpha\sim 0.2$) is seen to span several decades for all the values of μ. This is a remarkable example of universality generated by DOS fluctuations, completely absent in the KDM/DMFT treatment.

D. Distribution of the hybridization function

A key input to the determination of the Kondo temperature is the hybridization function $\Delta_f(i\omega_n)$ of Eq. (11). We show in Fig. 10(a) the distribution of its imaginary part calculated at the chemical potential ($i\omega_n\rightarrow 0-i\delta$). Note that, for a featureless bath, it appears in the exponential of the Kondo temperature formula, Eq. (18), which is thus very sensitive to it. It can be seen in Fig. 10(a) that its distribution

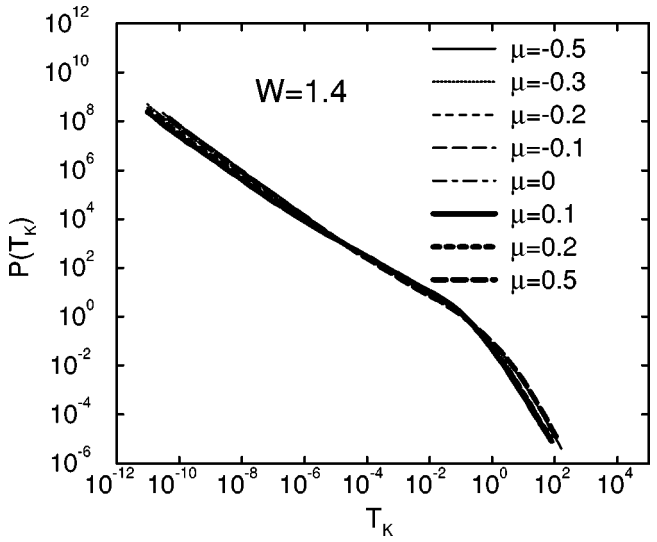

FIG. 9. Distribution of Kondo temperatures on a log-log scale, for different values of the chemical potential and fixed disorder $W=1.4$, using slave boson mean field theory as the impurity solver ($V=0.5$, $E_f=-1$).

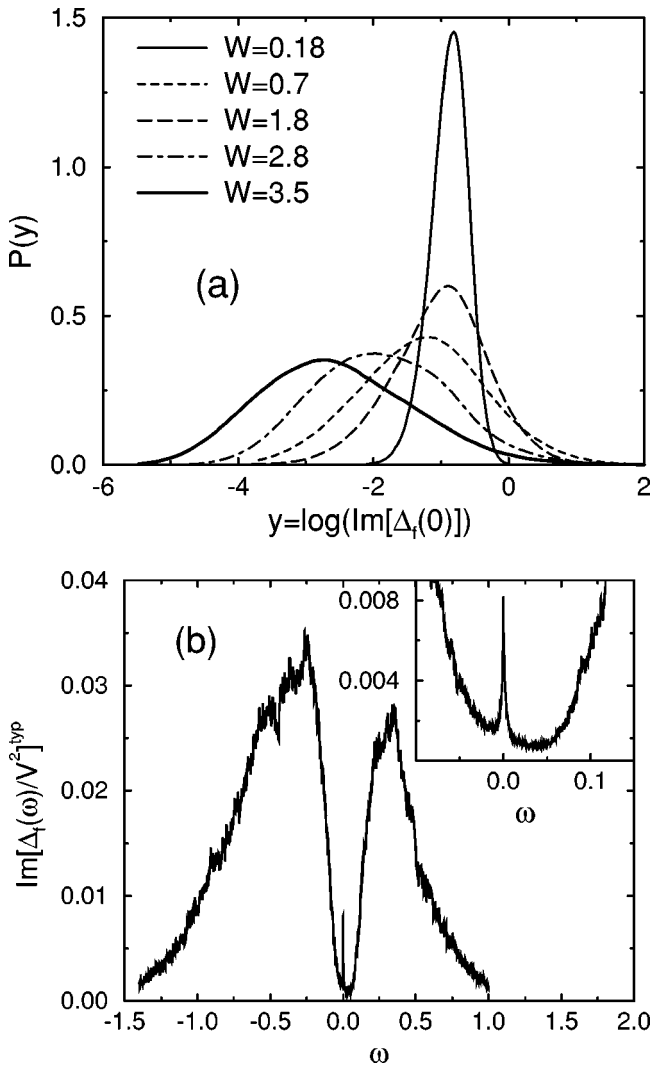

FIG. 10. (a) Distribution of the logarithm of $\mathrm{Im}[\Delta_f(0)]$ for different values of disorder and (b) typical value of $\mathrm{Im}[\Delta_f(\omega - i\delta)]$ as a function of frequency at $W=3.5$, both using slave boson mean field theory as the impurity solver. The inset in (b) details the behavior close to the chemical potential ($V=0.5$, $E_f=-1$, and $\mu=0.2$).

is very regular and retains a bell-shaped structure for any W. It also inherits the nonmonotonic behavior observed in the conduction electron local DOS [see Fig. 1(b)].

It is tempting to try to calculate the distribution of Kondo temperatures from the distribution of $\mathrm{Im}[\Delta_f(0-i\delta)]$, by naively applying the Kondo temperature formula, Eq. (18). This procedure fails, however: the actual distribution of T_K has a much lower weight at small T_K values than is predicted by the Kondo temperature formula. The explanation for this failure lies in the fact, already alluded to before, that T_K is determined by a weighted average of $\mathrm{Im}[\Delta_f(\omega-i\delta)]$ over a region around the Fermi level. This can be glimpsed from the strong frequency dependence of the *typical* (geometric average) hybridization function close to the chemical potential, as shown, for frequencies on the real axis, in Fig. 10(b). It shows a robust and well-defined pseudogap, inherited from the nearby Kondo insulator, and a tiny narrow peak at the chemical potential. This narrow peak is easy to understand: spatial fluctuations due to disorder give rise to narrow peaks within the pseudogap, most typically at the chemical potential. However, as we have remarked before, the Kondo temperature can be finite even if the density of states is zero or almost zero at the chemical potential.[65–67] In this case, the spectral weight right at the chemical potential is unimportant for the determination of the Kondo temperature. It is dominated by a whole range of spectral density away from the Fermi level. Since far from the pseudogap region the density of states is much larger and hence much less affected by the spatial fluctuations, the distribution of Kondo temperatures is narrower than one might guess based on the distribution of $\mathrm{Im}[\Delta_f(0-i\delta)]$ and the Kondo temperature formula.

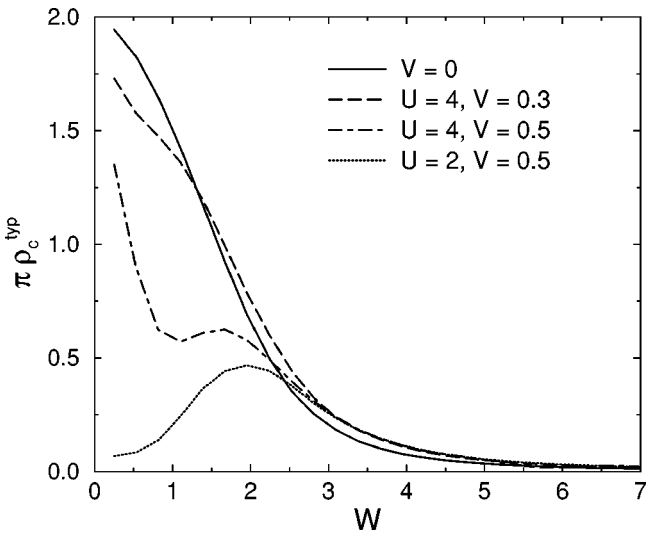

FIG. 11. Typical density of states near the Fermi surface as a function of disorder for different values of the hybridization V and the interaction U, using perturbation theory as the impurity solver. Other parameters used were $T=0.003$, $E_f=-1$, and $\mu=0$.

When considered together, the results of Sec. III show the importance of a self-consistent solution of the problem, with a nontrivial interplay between spatial fluctuations due to localization and strong correlation effects. However, an important feature that is missed in the slave boson treatment of the impurity problems is the presence of inelastic scattering. This will be considered in the next section, where we show the results obtained with perturbation theory in the interaction.

IV. PERTURBATION THEORY RESULTS

We now consider the results obtained at *finite* T using second-order perturbation theory as the impurity solver.

A. Results for a fixed temperature

Figure 11 shows the results for the conduction electron typical DOS near the Fermi level as a function of the disorder parameter W for different values of the interaction energy U and the hybridization V at $T=0.003$. In order to understand them, we looked at scatter plots of realizations of the local effective f-shell potential [real and imaginary parts of

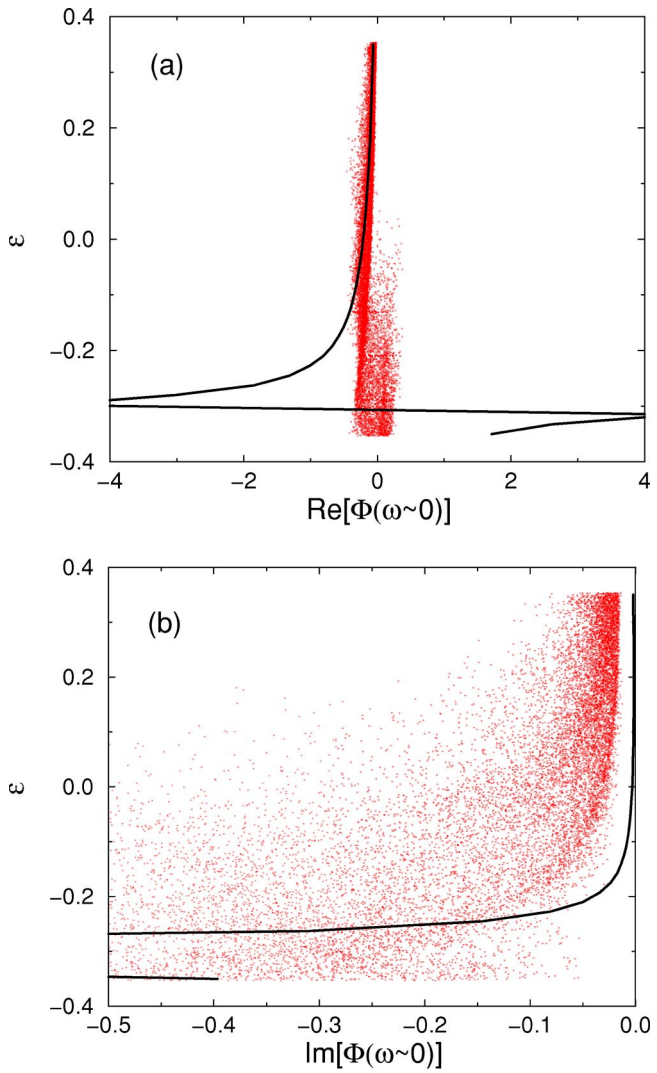

FIG. 12. Scatter plot of the effective f-shell potential $\Phi_j(\omega \approx 0)$ and the bare potential ϵ_j at the same site (dots) for $V=0.3$ and $W=0.7$, using perturbation theory as the impurity solver: (a) real and (b) imaginary parts. The solid line is the DMFT result for $W=0.7$. Other parameters used were $U=4$, $E_f=-1$, $T=0.003$, and $\mu=0$.

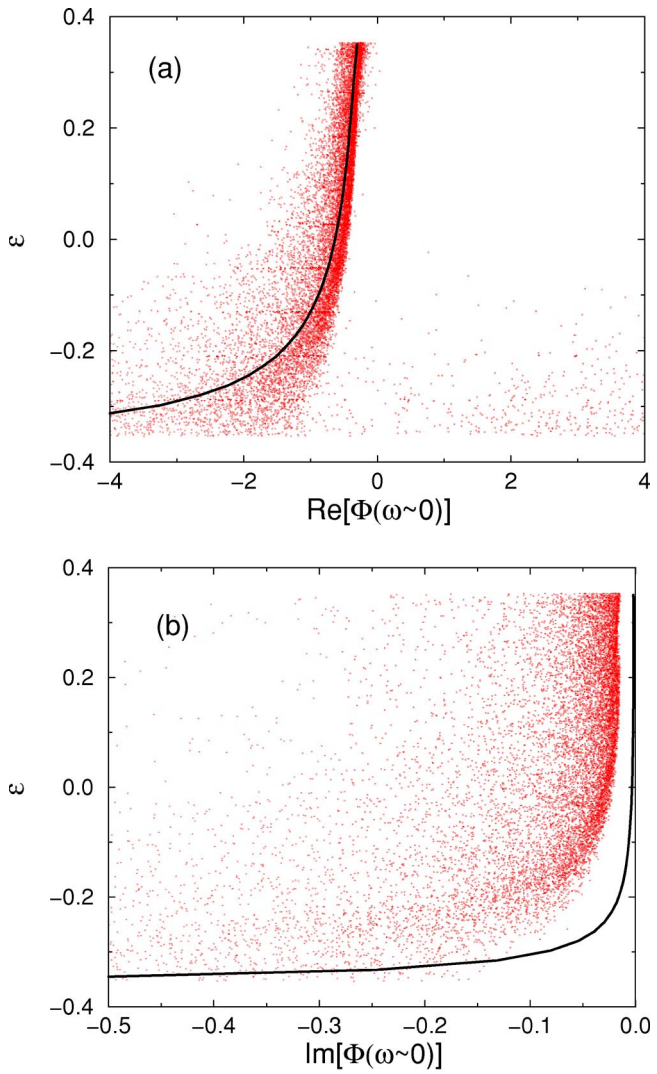

FIG. 13. Scatter plot of the effective f-shell potential $\Phi_j(\omega \approx 0)$ and the bare potential ϵ_j at the same site (dots) for $V=0.5$ and $W=0.7$, using perturbation theory as the impurity solver: (a) real and (b) imaginary parts. The solid line is the DMFT result for $W=0.7$. Other parameters as in Fig. 12.

$\Phi_j(\omega \approx 0)]$ and the corresponding bare potential ϵ_j at the same site, both seen by the conduction electrons. These results are presented for two different values of the hybridization $V=0.3$ and 0.5 and two different values of the disorder parameter $W=0.7$ and 7 in Figs. 12–15. The other parameters used in the calculation were $U=4$, $T=0.003$, $E_f=-1$, and $\mu=0$. The figures present the results obtained in the statDMFT calculation (represented by dots) as well as the results of DMFT (full line), in which the disorder treatment reduces to CPA.[17,16] It is important to notice that we have $\mathrm{Im}[\Phi(\omega \approx 0)] \neq 0$ {as $\mathrm{Im}[\Sigma_f(\omega \approx 0)] \neq 0$ at finite T}, implying the presence of *inelastic scattering*, a feature absent in the slave boson treatment of the last section. In addition, the imaginary part of the self-energy gets folded into the *real* part of $\Phi(\omega)$ as well. This is a peculiar feature of a two-band model, where the *effective* conduction electron self-energy represented by $\Phi(\omega)$ has a real part for which inelastic processes contribute. Thus, we should keep in mind that, even though in an effective description of conduction electron processes $\mathrm{Re}[\Phi_j(\omega \approx 0)]$ and ϵ_j are associated with elastic scattering while $\mathrm{Im}[\Phi_j(\omega \approx 0)]$ is related to inelastic processes, both $\mathrm{Re}[\Phi_j(\omega \approx 0)]$ and $\mathrm{Im}[\Phi_j(\omega \approx 0)]$ contain information on f-electron collisions.

Let us compare the results for $W=0.7$ for both $V=0.3$ and $V=0.5$, which are in Figs. 12 and 13. The first observation we make is that for $V=0.3$ the values of $\mathrm{Re}[\Phi(\omega \approx 0)]$ are mainly concentrated around zero, while for $V=0.5$ they are distributed in a wider range of values. On the other hand, the results for $\mathrm{Im}[\Phi(\omega \approx 0)]$ show that the inelastic scattering is stronger for $V=0.3$ than for $V=0.5$. Concerning the results for $V=0.5$, the great concentration of sites with large $\mathrm{Re}[\Phi(\omega \approx 0)]$ explains the great decrease in the typical DOS for low disorder shown in Fig. 11. These sites act as almost unitary scatterers, which give rise to a maximally allowed scattering phase shift ($\delta=\pi/2$) for the

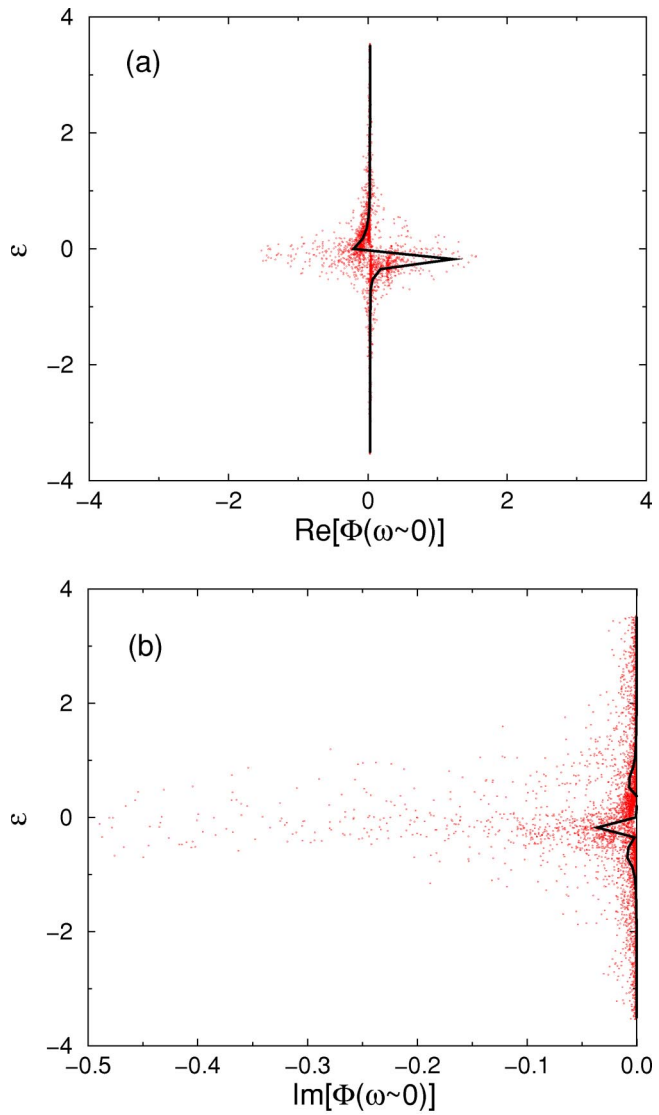

FIG. 14. Scatter plot of the effective f-shell potential $\Phi_j(\omega \approx 0)$ and the bare potential ϵ_j at the same site (dots) for $V=0.3$ and $W=7$, using perturbation theory as the impurity solver: (a) real and (b) imaginary parts. The solid line is the DMFT result for $W=7$. Other parameters as in Fig. 12.

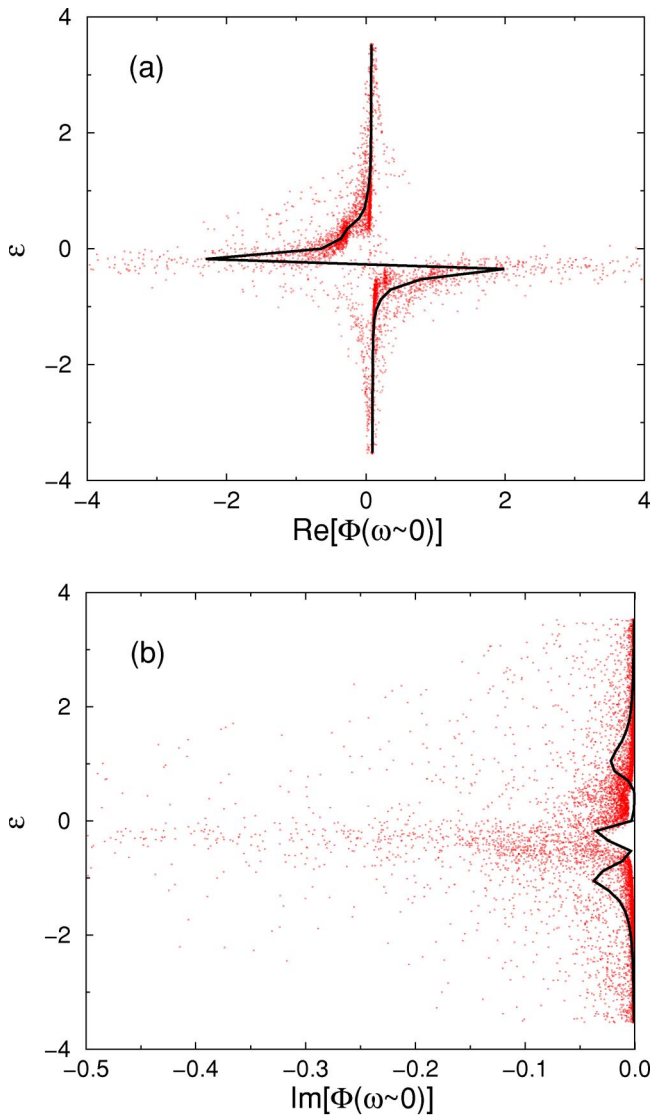

FIG. 15. Scatter plot of the effective f-shell potential $\Phi_j(\omega \approx 0)$ and the bare potential ϵ_j at the same site (dots) for $V=0.5$ and $W=7$, using perturbation theory as the impurity solver: (a) real and (b) imaginary parts. The solid line is the DMFT result for $W=7$. Other parameters as in Fig. 12.

conduction electrons, and represent droplets of Kondo insulator within the metal, in close parallel to the slave boson results discussed of Sec. III.[18,19] For $V=0.3$, although the inelastic scattering is stronger, it cannot compensate for the much narrower distribution of $\mathrm{Re}[\Phi(\omega \approx 0)]$. Thus, the DOS does not decrease as fast as for $V=0.5$.

As the disorder increases to intermediate values ($W \approx 1.8$), the distribution of ϵ becomes larger, causing a steady decrease in the typical DOS for $V=0.3$. However, for $V=0.5$, the typical DOS presents a nonmonotonic behavior similar to the slave boson results for $-0.3 \lesssim \mu \lesssim 0.1$ and $0.1 \lesssim \mu \lesssim 0.4$. As we explained in Sec. III, this is a result of the fact that, as the disorder increases, the concentration of unitary scatterers first increases, then saturates and the bare disorder dominates over the f-related one $[\Phi_j(\omega)]$.[18,19] Indeed, even for $V=0.3$ we notice the presence of a slight "shoulder" in the typical DOS around $W=1.1$, whose origin is the same as that of the non-monotonic behavior at $V=0.5$. We call attention to the slave boson results of Fig. 2, which similarly show that a decrease of the hybridization strength moves the "dip-hump" feature to smaller disorder values. Moreover, as the current calculation was done at finite temperature, inelastic scattering also plays some role in smoothing out this feature.

As the disorder continues to increase and the distribution of ϵ becomes broader, the typical DOS for both $V=0.3$ and $V=0.5$ decreases. These results tend to the noninteracting one, as is expected if only the bare disorder plays a role. Indeed, comparing the results for $W=7$ (Figs. 14 and 15) we notice that the realizations for which the bare disorder ϵ is large have $\mathrm{Re}[\Phi(\omega \approx 0)]$ around zero, meaning that the real part of the f-shell disorder is not important. In addition, the

values of $\mathrm{Im}[\Phi(\omega\approx 0)]$ are small for these realizations. In the case of the realizations for which ϵ is small, $\mathrm{Re}[\Phi(\omega\approx 0)]$ attains values that are larger than the results for $W=0.7$ (cf. Figs. 12 and 13).

The above discussion has focused on the conduction electron viewpoint. Let us now consider how the presence of disorder in ϵ is seen by the f electrons. For the auxiliary one-impurity problem, the important scale is the Kondo temperature T_K, which measures the coupling between the impurity and the conduction electron bath. The presence of disorder in ϵ generates a distribution of T_K, as we have seen before. Thus at finite temperature some of the sites have $T_K>T$, forming a singlet state with the bath, while the sites for which $T_K<T$ represent an almost free spin, scattering conduction electrons incoherently. This incoherence is characterized by a large amount of inelastic scattering, signaled by a significant imaginary part of the self-energy. Going back to the results for $W=0.7$, the fact that the inelastic scattering is stronger for $V=0.3$ than for $V=0.5$ reflects the larger number of incoherent sites (with $T_K<T$) in the former, since the smaller the hybridization, the smaller the Kondo temperature [see Eqs. (18) and (20)]. On the other hand, the sites with large $\mathrm{Re}[\Phi(\omega\approx 0)]$ for $V=0.5$, which are responsible for the great decrease in the typical DOS, represent sites with $T_K>T$.

Figure 11 also shows the results for the typical DOS for $U=2$ and $V=0.5$. In this case, the system has particle-hole symmetry in the clean limit, presenting a gap in its DOS (the Kondo insulator). This explains the fact that for small disorder the typical DOS decreases as W decreases. The overall behavior here bears strong similarity with the slave boson results of Fig. 1(a) (circles) and the explanation for it has been given in Sec. III.

B. Temperature dependence

Figure 16 presents the results for the typical DOS as a function of W for different temperatures. The other parameters used were $U=4$, $V=0.3$, $E_f=-1$, and $\mu=0$. Here is where the interplay between inelastic and elastic processes proves to be fairly nontrivial and the use of a technique that incorporates both, such as perturbation theory, is crucial. First we note that for the lowest disorder value ($W=0.25$), the typical DOS decreases with increasing temperature. This is made more clear in the inset. On the other hand, for $W=1.4$, this tendency is reversed. Finally, in between these two extremes, the temperature dependence can be nonmonotonic. A better sense of the overall behavior can be grasped by plotting the inverse of the typical DOS as a function of T for different values of W, as shown in Fig. 17. It is clear that for $0.7\leqslant W\leqslant 1.2$, the inverse typical DOS shows a peak as a function of T, which gradually moves to zero temperature as disorder is increased.

The temperature dependence of the typical DOS can be rationalized by looking at the corresponding changes in the distribution of $\Phi(\omega\approx 0)$. For this purpose, we focus on the disorder value of $W=0.7$, for which $1/\pi\rho_c^{\mathrm{typ}}$ has a clear maximum at $T\approx 0.0005$. We show in Figs. 18 and 19 the scatter plots of $\Phi(\omega\approx 0)$ at $T=0.0001$ and $T=0.0005$, respectively, which should be compared to the higher temperature results ($T=0.003$) of Fig. 12. From Fig. 17 we see that the inverse typical DOS increases as we go from $T=0.0001$ to $T=0.0005$ and then decreases as the temperature is varied up to $T=0.003$. As can be seen from the figures, this nonmonotonic behavior is governed by the effective f-disorder encoded in the distribution of $\mathrm{Re}[\Phi(\omega\approx 0)]$. Indeed, its variance increases from $T=0.0001$ to $T=0.0005$ but decreases from $T=0.0005$ to $T=0.003$. Note that the imaginary part of $\Phi(\omega\approx 0)$ always increases with increasing temperature, reflecting the enhancement of inelastic processes. In terms of T_K, this is the same as saying that as the temperature increases the number of sites with $T_K<T$, which have a stronger inelastic scattering, becomes larger. How-

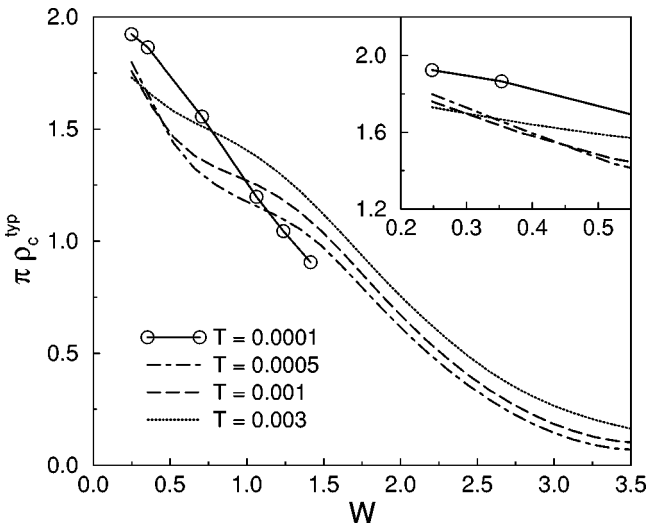

FIG. 16. Typical density of states near the Fermi surface as a function of disorder for different values of temperature, using perturbation theory as the impurity solver. Other parameters used were $U=4$, $V=0.3$, $E_f=-1$, and $\mu=0$.

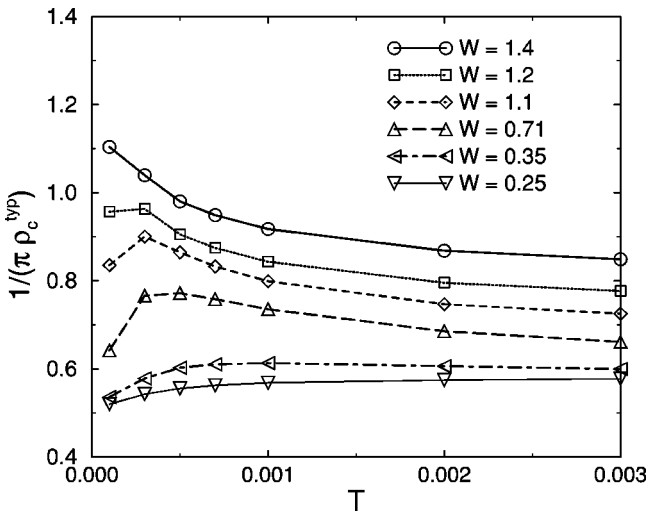

FIG. 17. Inverse typical density of states near the Fermi surface as a function of temperature for different values of disorder, using perturbation theory as the impurity solver. Other parameters as in Fig. 16.

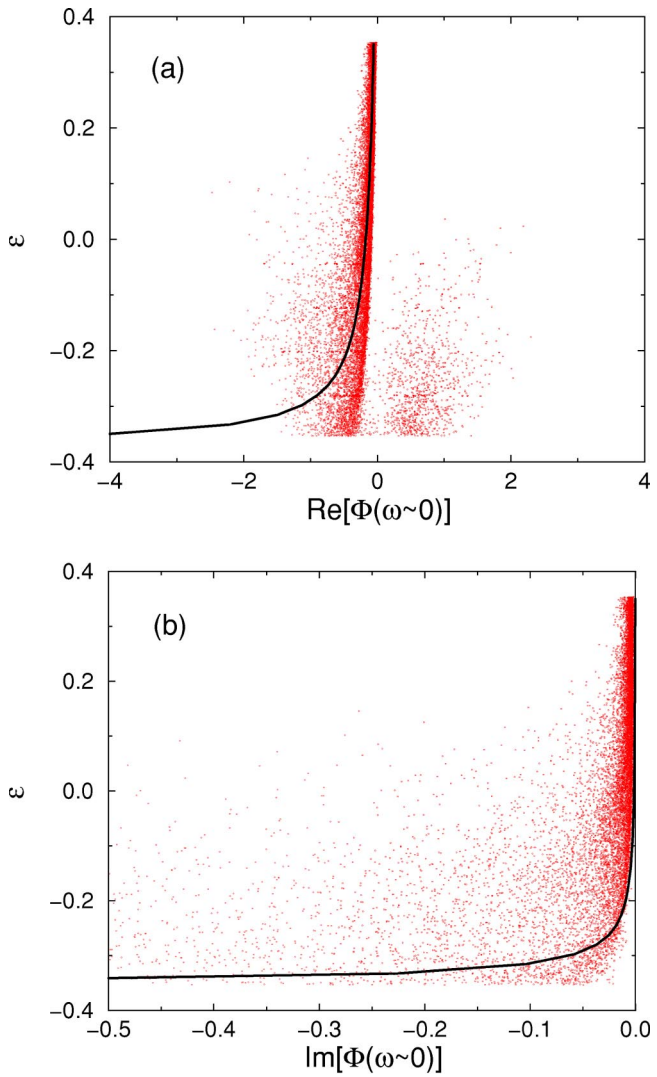

FIG. 18. Scatter plot of the effective f-shell potential $\Phi_j(\omega \approx 0)$ and the bare potential ϵ_j at the same site (dots) for $T=0.0005$ and $W=0.7$, using perturbation theory as the impurity solver: (a) real and (b) imaginary parts. The solid line is the DMFT result for $W=0.7$. Other parameters as in Fig. 16.

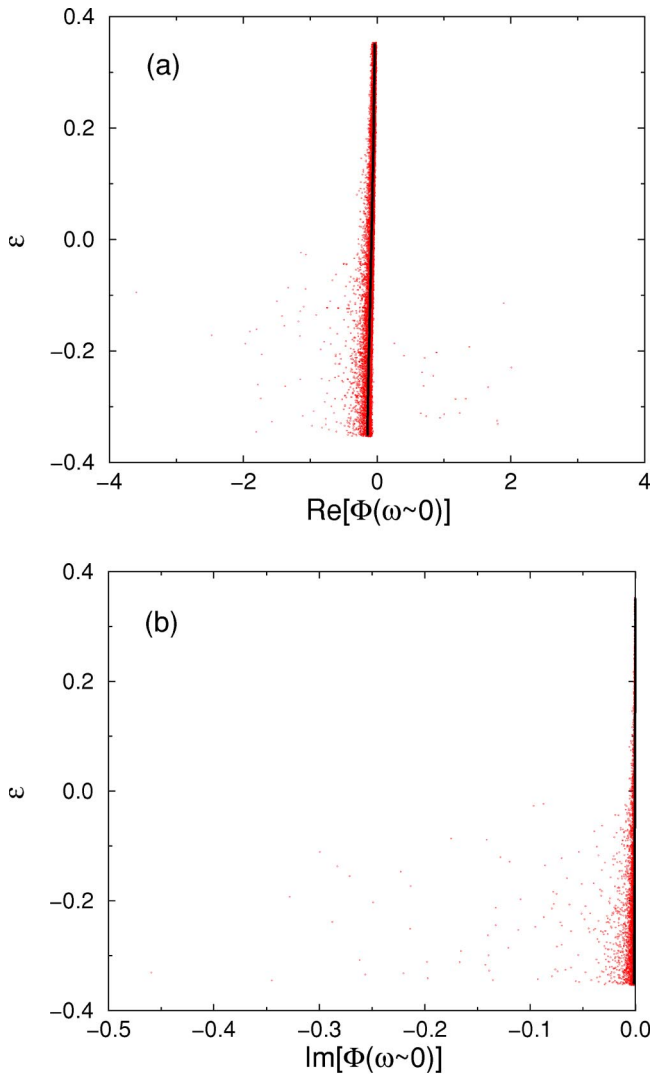

FIG. 19. Scatter plot of the effective f-shell potential $\Phi_j(\omega \approx 0)$ and the bare potential ϵ_j at the same site (dots) for $T=0.0001$ and $W=0.7$, using perturbation theory as the impurity solver: (a) real and (b) imaginary parts. The solid line is the DMFT result for $W=0.7$. Other parameters as in Fig. 16.

ever, in the interval from about $T=0.0005$ up to $T=0.003$, the increase of $\mathrm{Im}[\Phi(\omega \approx 0)]$ is *outweighed* by the narrowing of the distribution of $\mathrm{Re}[\Phi(\omega \approx 0)]$, which is the dominant contribution. The above analysis can be similarly extended to the other values of disorder shown in Fig. 17.

All along we have been using the typical DOS as a measure of the conducting properties of the system. This is justified by its interpretation as a escape rate from a lattice site and the fact that it vanishes at the localization transition.[61] Ideally, one would like to calculate the conductivity instead. This is a difficult task in the present scheme, however, although an approximate calculation can be performed, which becomes accurate close to the localization transition.[68,69] It requires the calculation of the propagator between two different sites, which goes beyond our current method, whose focus is on local Green's functions only. Even in view of all these caveats, however, it is tempting to use the inverse typical DOS as an approximate measure of the resistivity, especially far from the weakly disordered region ($W>0.35$). If this is done, then the fanning out of the "resistivity" curves of Fig. 17 as $T \to 0$ is reminiscent of the Mooij correlations,[23] originally observed in disordered transition metal alloys, but which are also seen in heavy fermion alloys,[70] doped Kondo insulators,[71–73] and even in two-dimensional systems as in the metal-oxide-semiconductor field-effect transistors.[1] Our results and the discussion above show that the interplay between localization effects and electron-electron interactions can give rise to the Mooij correlations, without the need to invoke other sources, such as electron-phonon interactions.[68,74] In addition, we have pointed out how the rapid drop in the typical DOS is a consequence of the proximity to the Kondo insulator, a region where localization effects are particularly large. Taken together, these observations point to a close connection between Mooij correlations and localization effects in the vicinity of a Kondo or a Mott insulator. It would be interesting to test these ideas by a

direct calculation of the resistivity within a scheme capable of incorporating both localization and strong correlations.

Finally, regarding the DMFT calculation presented in all the figures discussed in this section, we note that the results obtained for $\mathrm{Re}[\Phi(\omega\approx 0)]$ fall approximately in the region where the concentration of realizations in the statDMFT calculation is largest. There is no reason to expect DMFT and the statDMFT to give similar results, except at weak disorder. Nevertheless, our results show that, surprisingly, DMFT can serve as a rough guide for the most probable values of $\mathrm{Re}[\Phi(\omega\approx 0)]$. There is a sizeable discrepancy, however, between the DMFT and the statDMFT results for $\mathrm{Im}[\Phi(\omega\approx 0)]$ at the highest temperature ($T=0.003$) and low disorder. The DMFT line in this case is an underestimate of the realizations obtained within the statDMFT. As the temperature is lowered a better agreement is obtained. Thus, in addition to its inherent neglect of localization effects, DMFT should be used only as a lower bound when gauging the importance of inelastic processes in disordered Anderson lattices.

V. DISCUSSION AND CONCLUSIONS

We have in this paper extensively characterized the physics of disordered Anderson lattices within the statDMFT scheme, which is able to incorporate both localization effects and the local correlations coming from electron-electron interactions. This was done using both large-N methods and perturbation theory for the auxiliary single impurity problems. These are in a sense complementary approaches. On the one hand, large-N theory is ideal for ground state properties, where inelastic effects are absent. In particular, it affords a quick and reliable way of calculating Kondo temperatures (with the correct exponential dependence) and scattering phase shifts at $T=0$. Without $1/N$ corrections, however, it is unsuitable for a finite temperature calculation. On the other hand, second order perturbation theory has the advantage of being equally flexible with the added bonus of incorporating inelastic processes and the temperature dependence of the scattering phase shifts. Nevertheless, it fails to capture the exponential nature of the low-temperature scale of the single impurity problem. Taken together, the two methods have enabled us to put on firm grounds the conclusions laid out in previous work,[18,19] namely, the emergence of an electronic Griffiths phase in Anderson lattices governed by the proximity to the disorder-induced localization transition. In particular, several inadequacies of the early Kondo disorder model (and its formulation as a dynamical mean field theory) have been given a better theoretical basis once localization effects were included. The self-averaging effect introduced by the spatial fluctuations of the conduction electron wave functions induce a much higher degree of universality than is possible in the rigid KDM description. Furthermore, the perturbation theory treatment has also suggested a mechanism behind the ubiquitous observation of Mooij correlations in the resistivity of disordered materials.

Even within the confines of the approximations of the statDMFT scheme, there are still outstanding issues that we would like to resolve. Even though a fully analytical treatment is probably impossible, it might be feasible to devise an approximate parameterization of the statDMFT on the Bethe lattice, specially at weak disorder. In this respect, the universality of the distributions of ''dressed'' quantities, such as the various local Green's functions and the Kondo temperatures, which are either Gaussian or log normal is a useful guide. A ''toy'' model that assumes a simple form for the distribution of $\Delta_{cj}(i\omega_n)$ can be written down, which recovers the Griffiths singularities obtained in the numerical treatment.[75] This ''toy'' model may prove useful for a calculation of the resistivity and for generalizations of the statDMFT treatment.

On the other hand, a specially important effect neglected in the statDMFT is two-particle inter-site correlations, particularly in the spin channel. Indeed, the proliferation of poorly quenched low-T_K spins in our treatment generates a large amount of entropy that must be relieved at low temperatures through intersite correlations. Indeed, experimental evidence in favor of spin-glass dynamics at low temperatures in $UCu_{5-x}Pd_x$[45] and URh_2Ge_2[44] makes the inclusion of intersite correlations more pressing. A promising avenue of attack would be to remain true to the spirit of the DMFT and use its extended version. Several treatments along these lines have been attempted.[41,42,76] The challenge in our case is to incorporate both the dynamical intersite correlations of the latter treatments and the spatial fluctuations of Kondo temperatures of the electronic Griffiths phase we find in our approach. We defer the discussion of this problem to a future publication.

ACKNOWLEDGMENTS

We thank M. J. Rozenberg for useful discussions. We also thank C. H. Booth for providing us with his XAFS data. This work was supported by FAPESP through Grants No. 99/00895-9 (M.C.O.A.), 98/12741-3 (E.M.), 01/00719-8 (E.M.), by CNPq through Grant No. 301222/97-5 (E.M.), and by the NSF through Grants No. DMR-9974311 and NSF-0234215 (V.D.).

APPENDIX: BRIEF DESCRIPTION OF THE NUMERICAL METHOD

The set of stochastic equations defined in Eqs. (5)–(17) must be solved in two steps. First, action (5)–(8) is solved with the bath function with $z-1$ nearest neighbors defined in Eq. (17). This determines self-consistently the distribution of local conduction electron Green's functions with one nearest neighbor removed $G_{cl}^{\mathrm{loc}(j)}(i\omega_n)$. Next, the same action (5)–(8) is solved, this time with the bath function in (9), constructed from the previously determined $G_{cl}^{\mathrm{loc}(j)}(i\omega_n)$. This step involves no self-consistency and yields the distribution of $G_{cj}^{\mathrm{loc}}(i\omega_n)$ as output. Since the latter bath function is a sum over z nearest neighbors its statistical fluctuations are reduced compared to the former one. Thus, $G_{cj}^{\mathrm{loc}}(i\omega_n)$ is more narrowly distributed than $G_{cl}^{\mathrm{loc}(j)}(i\omega_n)$. Yet, we expect the qualitative behavior to be the same. We have therefore focused on the first step of the procedure only.

For a given impurity solver, this disordered Bethe lattice problem was solved for $z=3$, by sampling the distribution of $G_{cj}^{\mathrm{loc}(l)}(i\omega_n)$ from an ensemble of N sites, as proposed origi-

nally in Ref. 47. We have generally used $N=70-100$ since we have checked that the results do not change by taking $N=200$. We have thus determined the distribution of various local properties.

The equations were solved on a discrete mesh along the Matsubara axis. The mesh is set by the Matsubara frequencies in the perturbative treatment at finite temperatures and by an arbitrary finite discrete mesh in the slave boson mean field theory at $T=0$ (up to 32 000 points). The choice of the imaginary frequency axis is due to a greater numerical stability. When the disorder is strong, the various Green's functions show large fluctuations. However, these are much more pronounced on the real frequency axis, where they give rise to several peaks and gaps.

The slave boson treatment consists in finding the two mean field parameters q and ϵ_f by solving the set of two nonlinear Eqs. (25)–(26). For that, we used the Powell hybrid method. The integrals were calculated with standard adaptive quadrature routines. Since we used a finite frequency mesh, it was important to extrapolate the value of $G_f^{qp}(i\omega)$ with the asymptotic form $1/i\omega$ for values of ω greater than the largest mesh value. In this fashion, a wide range of Kondo temperatures is covered, going down to almost machine precision in the clean metallic case. When disorder is present a given impurity problem may not have a solution even at $T=0$, because the strong spatial fluctuations may cause the local DOS to vanish at the Fermi level. In this case, there are two possible regimes for the impurity, which have been carefully analyzed.[65–67] The analysis shows that there is a critical coupling constant V_c such that the ground state is a singlet for $V>V_c$ (the so-called "strong coupling Kondo effect"), whereas the local moment remains unquenched if $V<V_c$. When a solution could not be found, this corresponded to either a free spin ($V<V_c$) or a Kondo temperature which is smaller than the smallest value we can reach with our numerical code. In either case, we set $q=0$, effectively decoupling the free moment from the rest of the lattice. Yet, we were still able to span several decades of energy scales.

In the perturbative treatment, the solution of each impurity problem is found by solving a set of two nonlinear equations for n and $\tilde{\mu}$, which is defined by Eqs. (30) and (35). As in the slave boson treatment we used the Powell hybrid method. The calculation of the second order correction for the self-energy involves Fourier transforms as, according to Eq. (31), it has a simpler form in imaginary time rather than in frequency space. For this, we used the fast Fourier transform algorithm.[77]

[1] E. Abrahams, S. V. Kravchenko, and M. P. Sarachick, Rev. Mod. Phys. **73**, 251 (2001).
[2] G. R. Stewart, Rev. Mod. Phys. **73**, 797 (2001).
[3] H. v. Löhneysen, T. Pietrus, G. Portisch, H. G. Schlager, A. Schröder, M. Sieck, and T. Trappmann, Phys. Rev. Lett. **72**, 3262 (1994).
[4] F. M. Grosche, S. R. Julian, N. D. Mathur, and G. G. Lonzarich, Physica B **223-224**, 50 (1996).
[5] A. Schröder, G. Aeppli, E. Bucher, R. Ramazashvili, and P. Coleman, Phys. Rev. Lett. **80**, 5623 (1998).
[6] N. D. Mathur, F. M. Grosche, S. R. Julian, I. R. Walker, D. M. Freye, R. K. W. Haselwimmer, and G. G. Lonzarich, Nature (London) **394**, 39 (1998).
[7] A. Rosch, Phys. Rev. Lett. **82**, 4280 (1999).
[8] J. A. Hertz, Phys. Rev. B **14**, 1165 (1976).
[9] M. A. Continentino, G. M. Japiassu, and A. Troper, Phys. Rev. B **39**, 9734 (1989).
[10] A. J. Millis, Phys. Rev. B **48**, 7183 (1993).
[11] Q. Si, S. Rabello, K. Ingersent, and J. L. Smith, Nature (London) **413**, 804 (2001).
[12] B. Andraka and G. R. Stewart, Phys. Rev. B **47**, 3208 (1993).
[13] O. O. Bernal, D. E. MacLaughlin, H. G. Lukefahr, and B. Andraka, Phys. Rev. Lett. **75**, 2023 (1995).
[14] T. Taniguchi, Y. Tabata, and Y. Miyako, J. Phys. Soc. Jpn. **68**, 2026 (1999).
[15] Y. Tabata, D. R. Grempel, M. Ocio, T. Taniguchi, and Y. Miyako, Phys. Rev. Lett. **86**, 524 (2000).
[16] E. Miranda, V. Dobrosavljević, and G. Kotliar, Phys. Rev. Lett. **78**, 290 (1997).
[17] E. Miranda, V. Dobrosavljević, and G. Kotliar, J. Phys.: Condens. Matter **8**, 9871 (1996).
[18] E. Miranda and V. Dobrosavljević, Phys. Rev. Lett. **86**, 264 (2001).
[19] E. Miranda and V. Dobrosavljević, J. Magn. Magn. Mater. **226-230**, 110 (2001).
[20] R. Griffiths, Phys. Rev. Lett. **23**, 17 (1969).
[21] N. Read and D. M. Newns, J. Phys. C **16**, L1055 (1983).
[22] P. Coleman, Phys. Rev. B **35**, 5072 (1987).
[23] J. H. Mooij, Phys. Status Solidi A **17**, 521 (1973).
[24] A. Georges, G. Kotliar, W. Krauth, and M. J. Rozenberg, Rev. Mod. Phys. **68**, 13 (1996).
[25] E. N. Economou, *Green's Functions in Quantum Physics* (Springer, Berlin, 1983), p. 141.
[26] A. Chattopadhyay and M. Jarrell, Phys. Rev. B **56**, 2920 (1997).
[27] A. Chattopadhyay, M. Jarrell, and H. R. Krishnamurthy, cond-mat/9805127 (1998) unpublished.
[28] D. E. MacLaughlin *et al.*, Physica B **289-290**, 15 (2000).
[29] N. Büttgen, W. Trinkl, J.-E. Weber, J. Hemberger, A. Loidl, and S. Kehrein, Phys. Rev. B **62**, 11 545 (2000).
[30] C. H. Booth, E.-W. Scheidt, U. Killer, A. Weber, and S. Kehrein, Phys. Rev. B **66**, 140402 (2002).
[31] V. Dobrosavljević, T. R. Kirkpatrick, and B. G. Kotliar, Phys. Rev. Lett. **69**, 1113 (1992).
[32] C. H. Booth, D. E. MacLaughlin, R. H. Heffner, R. Chau, M. B. Maple, and G. H. Kwei, Phys. Rev. Lett. **81**, 3960 (1998).
[33] E. D. Bauer, C. H. Booth, G. H. Kwei, R. Chau, and M. B. Maple, Phys. Rev. B **65**, 245114 (2002).
[34] V. Dobrosavljević and G. Kotliar, Phys. Rev. Lett. **78**, 3943 (1997).
[35] V. Dobrosavljević and G. Kotliar, Philos. Trans. R. Soc. London, Ser. A **356**, 57 (1998).

[36] A. H. Castro Neto, G. Castilla, and B. A. Jones, Phys. Rev. Lett. **81**, 3531 (1998).
[37] M. C. de Andrade *et al.*, Phys. Rev. Lett. **81**, 5620 (1998).
[38] A. H. Castro Neto and B. A. Jones, Phys. Rev. B **62**, 14 975 (2000).
[39] A. J. Millis, D. K. Morr, and J. Schmalian, Phys. Rev. B **66**, 174433 (2002).
[40] S. Sachdev, N. Read, and R. Oppermann, Phys. Rev. B **52**, 10 286 (1995).
[41] A. M. Sengupta and A. Georges, Phys. Rev. B **52**, 10 295 (1995).
[42] D. R. Grempel and M. J. Rozenberg, Phys. Rev. B **60**, 4702 (1999).
[43] R. Vollmer, T. Pietrus, H. v. Löhneysen, R. Chau, and M. B. Maple, Phys. Rev. B **61**, 1218 (2000).
[44] S. Süllow, G. J. Nieuwenhuys, A. A. Menovsky, J. A. Mydosh, S. A. M. Mentink, T. E. Mason, and W. J. L. Buyers, Phys. Rev. Lett. **78**, 354 (1997).
[45] D. E. MacLaughlin, O. O. Bernal, R. H. Heffner, G. J. Nieuwenhuys, M. S. Rose, J. E. Sonier, B. Andraka, R. Chau, and M. B. Maple, Phys. Rev. Lett. **87**, 066402 (2001).
[46] Y. Yamamoto *et al.*, Physica B **259-261**, 66 (1999).
[47] R. Abou-Chacra, P. W. Anderson, and D. J. Thouless, J. Phys. C **6**, 1734 (1973).
[48] G. Zaránd and L. Udvardi, Phys. Rev. B **54**, 7606 (1996).
[49] A. C. Hewson, *The Kondo Problem to Heavy Fermions* (Cambrige University Press, Cambridge, 1993).
[50] K. Yosida and K. Yamada, Prog. Theor. Phys. **46**, 244 (1970).
[51] K. Yamada, Prog. Theor. Phys. **53**, 970 (1975).
[52] K. Yosida and K. Yamada, Prog. Theor. Phys. **53**, 1286 (1975).
[53] K. Yamada, Prog. Theor. Phys. **54**, 316 (1975).
[54] V. Zlatić and B. Horvatić, Phys. Rev. B **28**, 6904 (1983).
[55] J. Ferrer, A. Martín-Rodero, and F. Flores, Phys. Rev. B **36**, 6149 (1987).
[56] H. Kajueter and G. Kotliar, Phys. Rev. Lett. **77**, 131 (1996).
[57] M. Potthoff, T. Wegner, and W. Nolting, Phys. Rev. B **55**, 16 132 (1997).
[58] T. Wegner, M. Potthoff, and W. Nolting, Phys. Rev. B **57**, 6211 (1998).
[59] D. Meyer and W. Nolting, Phys. Rev. B **61**, 13 465 (2000).
[60] D. Meyer and W. Nolting, Phys. Rev. B **62**, 5657 (2000).
[61] P. W. Anderson, Phys. Rev. **109**, 1492 (1958).
[62] A. D. Mirlin and Y. V. Fyodorov, Nucl. Phys. B **366**, 507 (1991).
[63] G. Aeppli and Z. Fisk, Comments Condens. Matter Phys. **16**, 155 (1992).
[64] P. S. Riseborough, Adv. Phys. **49**, 257 (2000).
[65] V. Dobrosavljević and G. Kotliar, Phys. Rev. B **46**, 5366 (1992).
[66] K. Takegahara, Y. Shimizu, and O. Sakai, J. Phys. Soc. Jpn. **61**, 3443 (1992).
[67] K. Ingersent, Phys. Rev. B **54**, 11 936 (1996).
[68] S. M. Girvin and M. Jonson, Phys. Rev. B **22**, 3583 (1980).
[69] V. Dobrosavljević, A. A. Pastor, and B. K. Nikolić, Europhys. Lett. **62**, 76 (2003).
[70] C. L. Lin, A. Wallash, J. E. Crow, T. Mihalisin, and P. Schlottmann, Phys. Rev. Lett. **58**, 1232 (1987).
[71] J. F. DiTusa, K. Friemelt, E. Bucher, G. Aeppli, and A. P. Ramirez, Phys. Rev. Lett. **78**, 2831 (1997).
[72] J. F. DiTusa, K. Friemelt, E. Bucher, G. Aeppli, and A. P. Ramirez, Phys. Rev. Lett. **78**, 4309(E) (1997).
[73] J. F. DiTusa, K. Friemelt, E. Bucher, G. Aeppli, and A. P. Ramirez, Phys. Rev. B **58**, 10 288 (1998).
[74] P. A. Lee and T. V. Ramakrishnan, Rev. Mod. Phys. **57**, 287 (1985).
[75] V. Dobrosavljević and E. Miranda (unpublished).
[76] S. Burdin, D. R. Grempel, and A. Georges, Phys. Rev. B **66**, 045111 (2002).
[77] W. H. Press, B. P. Flannery, S. A. Teukolsky, and W. T. Vetterling, *Numerical Recipes in Fortran*, 2nd ed. (Cambridge University Press, 1992).